

Enhancing data-limited assessments with random effects:

A case study on Korea chub mackerel (*Scomber
japonicus*)

Kyuhan Kim^{1*}, Nokuthaba Sibanda², Richard Arnold²,

Teresa A'mar^{1,3}

*Corresponding author: kh2064@gmail.com

¹Dragonfly Data Science, PO Box 27535, Wellington 6141, New Zealand

²School of Mathematics and Statistics, Victoria University of Wellington, PO Box 600, Wellington 6140, New Zealand

³Current affiliation: Meridian Energy Limited, PO Box 10840, Wellington 6143, New Zealand

Abstract

In a state-space framework, temporal variations in fishery-dependent processes can be modeled as random effects. This modeling flexibility makes state-space models (SSMs) powerful tools for data-limited assessments. Though SSMs enable the model-based inference of the unobserved processes, their flexibility can lead to overfitting and non-identifiability issues. To address these challenges, we developed a suite of state-space length-based age-structured models and applied them to the Korean chub mackerel (*Scomber japonicus*) stock. Our research demonstrated that incorporating temporal variations in fishery-dependent processes can rectify model mis-specification but may compromise robustness, which can be diagnosed through a series of model checking processes. To tackle non-identifiability, we used a non-degenerate estimator, implementing a gamma distribution as a penalty for the standard deviation parameters of observation errors. This penalty function enabled the simultaneous estimation of both process and observation error variances with minimal bias, a notably challenging task in SSMs. These results highlight the importance of model checking and the effectiveness of the penalized approach in estimating SSMs. Additionally, we discussed novel assessment outcomes for the mackerel stock.

Keywords: Chub mackerel, CPUE standardization, random effect, stock assessment, state-space model

Introduction

Trade-off between model complexity and data availability

Fisheries management faces many challenges, especially when dealing with fish stocks that have limited data available. In these cases, we often rely on fishery-dependent information, primarily catch-per-unit-effort (CPUE) data, as our primary source of information (Maunder and Punt, 2004; Maunder et al., 2006; Hoyle et al., 2024). However, CPUE is inherently subject to various influences, such as fluctuations in fishing efficiency, variations in environmental conditions, changes in fish availability to fishing gear, and shifts in the geographic scope of fishing grounds (Maunder and Punt, 2004; Maunder et al., 2006; Wilberg et al., 2009; Hoyle et al., 2024). These inherent variations in CPUE render it unreliable as an index of abundance without proper adjustments (Maunder and Punt, 2004; Maunder et al., 2006; Hoyle et al., 2024).

As a result, CPUE standardization has become standard practice in fisheries stock assessment. Over time, several approaches have been developed for standardizing CPUE data, including generalized linear models, generalized additive models, and generalized linear mixed models (Maunder and Punt, 2004; Wilberg et al., 2009; Hoyle et al., 2024). However, many of these methods require supplementary data, including information about when and where fishing activities occur, vessel specifications, environmental conditions, and the composition of the target species. Unfortunately, many fish stocks, particularly those newly brought under management, lack this supplementary information, making the application of standardization methods impractical for these stocks. Furthermore, these standardization models can only account for explicitly included factors, potentially leaving CPUE data vulnerable to unexplained influences (Wilberg et al., 2009).

In situations where auxiliary information for standardization is unavailable, an alternative approach to address unexplained variation in CPUE is to employ CPUE standardization models

within a stock assessment framework. This approach is similar to the methods described in Maunder (2001) and Maunder and Langley (2004), but with a shift toward using descriptive models instead of functional models. These descriptive models allow for temporal variation without explicitly specifying the underlying mechanism (Wilberg and Bence, 2006; Wilberg et al., 2009). While this approach involves estimating additional parameters, potentially leading to challenges such as over-parameterization and non-identifiability (Auger-Méthé et al., 2016, 2021; Hyun and Kim, 2022; Kim, 2022), adopting a state-space framework where temporal variations are treated as random effects (Nielsen and Berg, 2014; Miller et al., 2016; Miller and Hyun, 2018; Trijoulet et al., 2020; Stock and Miller, 2021; Kim, 2022) can help mitigate these issues (Punt, 2023).

In a state-space framework, unexplained variation in CPUE can be modeled as random effects. The relationship between CPUE and actual fish abundance is generally influenced by fishery-dependent factors such as selectivity (including components such as availability and contact selectivity) and fishing efficiency, which are not time-invariant in practice (Hoyle et al., 2024). Thus, the investigation of time-varying selectivity and catchability within assessment models has been explored in previous studies (Wilberg et al., 2009; Martell and Stewart, 2014; Punt et al., 2014). These studies suggested that integrating time-varying selectivity and catchability into assessment models can enhance performance and alleviate retrospective patterns — systematic changes in population size estimates or other derived quantities resulting from the addition or removal of recent data points (Wilberg and Bence, 2006; Martell and Stewart, 2014; Hurtado-Ferro et al., 2015). However, this approach, while more parsimonious than conventional fixed-effects models, introduces additional model parameters, potentially leading to robustness issues (Deroba et al., 2015).

Addressing time-varying factors through random effects requires estimating multiple variance parameters, a task complicated by non-identifiability issues that can arise in state-space models (Auger-Méthé et al., 2016, 2021). Even simple models encounter this problem, as

estimates often approach zero when attempting to estimate both observation and process error variance parameters (Auger-Méthé et al., 2016; Hyun and Kim, 2022; Kim, 2022). This issue becomes more pronounced in assessment models with multiple variance parameters (Kim, 2022). To confront this challenge, previous studies have employed various strategies, such as incorporating observation error variance as an input (Miller et al., 2016; Miller and Hyun, 2018; Trijoulet et al., 2020), assuming that observation and process error variances are equal (Ono et al., 2012; Parent and Rivot, 2012; Thorson and Minto, 2015; Rankin and Lemos, 2015), or imposing prior distributions on the observation and process error variance parameters (Pedersen and Berg, 2017; Stock and Miller, 2021; ICES, 2023). However, these approaches may yield biased estimates if the assumed values are inaccurate or if reliable prior information is unavailable. A potential solution is to use a non-degenerate estimator, which involves maximizing the marginal likelihood with a gamma distribution as a penalty function for parameters with boundary estimates, similar to applying a weakly informative gamma prior in Bayesian analysis (Chung et al., 2013; Gelman et al., 2020). While this approach is recommended in the Bayesian framework (Gelman et al., 2020), its practical performance in fisheries stock assessments remains unexplored, raising questions about its applicability and efficacy.

Main objectives of this study

In this study, we developed a length-based age-structured model in a state-space framework, where time-varying selectivity and catchability were incorporated. The model was designed to address unexplained temporal variability in CPUE when additional information for standardization is unavailable. We applied the model to the Korean mackerel (*Scomber japonicus*) stock as a case study. We chose the mackerel stock as a case study because the stock has been influenced by various fishery-dependent factors, including changes in fishing efficiency and fishing grounds (Lee and Kim, 2011; Seo et al., 2017). One potential issue with the mackerel stock is that CPUE has increased since 1985, but the reasons for this

increase are not well understood and have not been accounted for in stock assessments. Without a clear understanding of the factors driving the increase in CPUE, the common assumption that CPUE is proportional to abundance may not hold, potentially leading to overly optimistic stock assessment results. To the best of our knowledge, detailed information on fishery behavior for this mackerel stock, essential for CPUE data standardization, has not been recorded or is not in an accessible form. This absence of information is evident, as all recent published quantitative assessments of this stock have used the CPUE data without standardization (Jung, 2019; Gim, 2019; Gim et al., 2020; Jung et al., 2021b; Hong et al., 2022; Gim and Hyun, 2022; Kim, 2022; Gim, 2023). Despite the incomplete understanding of the influence of fishery-dependent factors on the assessment results, the stock has been managed using a quota-based system since 1999 (Sim et al., 2020; Hyun, 2023; Korea Fisheries Resources Agency, 2023).

Such limited understanding and information regarding fishery-dependent processes in the mackerel stock pose a significant challenge in providing robust and reliable stock assessment estimates. This challenge raises critical questions about the scientific foundation of the quota management system in Korea (Hyun, 2023). Our primary objective is to investigate potential time-varying components of fishery-dependent factors, specifically catchability and selectivity, under the data-limited conditions that the mackerel stock is currently facing. Our focus is on maintaining the statistical robustness of the model in terms of parameter identifiability (while estimating both process and observation variance parameters, which is often problematic in state-space models, as discussed above) and the validity of model assumptions while keeping the model as realistic as possible to reflect the time-varying nature of fishery-dependent factors. Additionally, we aim to understand how these time-varying components influence assessment results.

To validate the effectiveness of our proposed model, we conducted a comprehensive evaluation under various assumptions related to selectivity and catchability. Through an extensive

simulation study, we assessed the model's performance, examining aspects such as robustness, uncertainties, and biases. To validate assumptions associated with random effects, we examined goodness-of-fit of the model using a residual analysis. Moreover, we compared the model's performance with and without the non-degenerate estimator. This comparative analysis allowed us to investigate the efficacy of the penalized likelihood approach in addressing non-identifiability issues within state-space stock assessment models.

Materials and methods

In this section, we describe the data and methods used in this study. We first provide background information on the chub mackerel stock in Korean waters for better understanding of the data and model structure. We then describe the data used in this study, followed by the model structure, estimation procedure, and model checking processes. The notation used in this study is summarized in Table 1.

Background information on the mackerel stock

Government-issued quotas for the total allowable catch (TAC) have regulated the chub mackerel stock in Korean waters, with a specific focus on the large purse seine (LPS) fishery since 1999 (Korea Fisheries Resources Agency, 2023). Despite historical records indicating the presence of more than six different fisheries targeting the mackerel stock (e.g., large purse seine, small purse seine, gillnet, trawl, etc.), the LPS fishery alone contributes to over 90% of the annual total catch of chub mackerel in Korea (Jung, 2019).

The Korean National Institute of Fisheries Science (NIFS) has been collecting CPUE data since 1976 (Jung, 2019). For the computation of CPUE, NIFS collected data on catch (in weight) and effort from approximately 70% of all fishing trips undertaken by the LPS fishery annually. The harvesters involved in these trips were responsible for providing their catch and effort, with the latter measured in terms of the number of hauls (Jung, 2019).

In addition to the CPUE data, NIFS has collected samples of fish from landed catches by the LPS fishery to obtain biological parameters, including length, weight, and sexual maturity (Kim et al., 2020). While length and weight of the samples have been periodically measured, age determination has been rarely conducted (Kang et al., 2015; Jung et al., 2021a). Length frequency data from the LPS fishery have also been collected since 2000 (Kim et al., 2018; Gim, 2019).

To establish a scientific foundation for the TAC-based management of this stock, numerous prior studies have evaluated the mackerel stock using the aforementioned fishery-dependent data. However, all these previous studies made the assumption that the nominal CPUE data were directly proportional to the abundance of the stock (Jung, 2019; Gim, 2019; Gim and Hyun, 2019; Gim et al., 2020; Jung et al., 2021b; Hong et al., 2022; Gim and Hyun, 2022; Kim, 2022), relying on a single constant catchability parameter. Furthermore, when structured models were employed, it was assumed that selectivity remained constant over time (Gim, 2019; Gim and Hyun, 2019; Gim et al., 2020; Gim and Hyun, 2022; Kim, 2022).

These assumptions persisted, despite earlier studies discussing the temporal increase in vessel power in the LPS fishery (Seo et al., 2017) and temporal changes in its fishing locations (Lee and Kim, 2011). Ignoring these factors in CPUE data used for stock assessments could result in biased estimates of stock abundance due to potential hyperstability (Hilborn and Walters, 1992).

Data

As in previous studies that used structured population dynamics models (Gim et al., 2020; Gim and Hyun, 2022; Kim, 2022; Gim, 2023), this research utilized three datasets: CPUE data from 1976 to 2019, length composition data from 2000 to 2017, and annual catch (in weight) data from 1950 to 2021 (Fig. 1). The CPUE and length composition data were not available in a numerical form, so we extracted them from earlier publicly accessible

studies (Kim et al., 2018; Jung, 2019; Gim, 2019) by digitizing their published figures using WebPlotDigitizer (a process often referred to as reverse engineering) (Rohatgi, 2022). The accuracy of the digitized data was verified by comparing them with the original figures. Annual catch data were sourced from Statistics Korea (1976 to 2021) and the FishStatJ database (1950 to 1975) provided by the Food and Agriculture Organization of the United Nations (FAO) (FishstatJ, 2020).

Process models

We developed a length-based age-structured model as the primary process model to estimate the abundance of the chub mackerel stock. Within this model, we explored several descriptive models for catchability and selectivity. Our approach is akin to previous studies by Wilberg and Bence (2006) and Wilberg et al. (2009), where different modeling approaches for time-varying catchability were tested. However, we extended this approach to include time-varying selectivity as well.

This methodology allowed us to investigate potential time-varying components of these two fishery-dependent factors without requiring additional information on the underlying mechanisms. Further details on each model component are provided in the subsequent sections.

Population dynamics

The estimation of abundance for ages and years was conducted through an age-structured population dynamics model. Within this model, annual recruitment was assumed to be independent of the spawning stock biomass (SSB) as in previous studies (Szuwalski et al., 2015; Hilborn et al., 2017; Miller and Hyun, 2018). This assumption was also supported by Hiyama et al. (2002), who found no significant correlation between annual recruitment and SSB of chub mackerel in the adjacent waters of Japan.

We assumed a recruitment age of 0, as suggested by the catch-at-age estimates presented in Jung et al. (2021a). In their study, the authors developed an age-length key table using catch samples from the LPS fishery in 2015. This table was used to categorize the 2015 catch into distinct age classes. However, it should be noted that we did not incorporate this single age-length key table into our study. This decision was due to its year-specific nature, with detailed explanations provided in the *Length-at-age distributions in catch* section below.

The natural logarithm of the annual recruitment $\log(N_{0,t})$ was assumed to follow a normal distribution with a mean of $\log(R)$ and a variance of σ_R^2 . Thus, the annual abundance of age a in year t was calculated as follows:

$$N_{a,t} = \begin{cases} R \cdot e^{\varepsilon_t^R}, & \text{for } a = 0 \\ N_{a-1,t-1} \cdot e^{-Z_{a-1,t-1}}, & \text{for } 0 < a < A \\ N_{a-1,t-1} \cdot e^{-Z_{a-1,t-1}} + N_{a,t-1} \cdot e^{-Z_{a,t-1}}, & \text{for } a = A \end{cases}$$

Here, subscripts a and t represent the indices for age and year, respectively. $N_{a,t}$ represents the abundance (in numbers) of age a in year t . ε_t^R denotes the recruitment deviation in year t with a variance of σ_R^2 . $Z_{a,t}$ represents the total mortality rate for fish of age a in year t , which is the summation of the fishing mortality $F_{a,t}$ and the constant natural mortality M (i.e., $Z_{a,t} = F_{a,t} + M$). Finally, A represents the terminal age class, referred to as “the plus group,” where fish that are the same age or older are aggregated. Jung et al. (2021a) showed that ages from 0 to 5 constituted the majority of the catch in 2015 from their age-length key analysis, where a small number of otolith samples (7 out of 401) were estimated to be age of 6 and the growth increment between ages 5 and 6 was negligible. Therefore, we assumed the terminal age class to be 5. The natural mortality rate M was set to a fixed value of 0.53, which corresponds to the median estimate of the natural mortality rate for chub mackerel based on a review of various studies conducted by the Technical Working Group of the North Pacific Fisheries Commission (Nishijima et al., 2021). The initial abundance of age a (i.e.,

year $t = 1950$) was assumed to be at near unfished equilibrium (denoted as $N_{a,0}$), given that the catch for the initial two decades was minimal compared to the later years of the time series (Fig. 1a). The equation describing this initial abundance is provided in Appendix A. According to the separability assumption (Doubleday, 1976), the age-dependent fishing mortality $F_{a,t}$ was calculated as the product of the fully selected fishing mortality rate F_t (i.e., $F_t = \max(F_{a,t})$) and the age-dependent selectivity $S_{a,t}$:

$$F_{a,t} = F_t \cdot S_{a,t}.$$

The fully selected fishing mortality rate F_t was modeled using a random walk process in log space (Nielsen and Berg, 2014):

$$\log(F_t) = \begin{cases} \log(F_0) + \varepsilon_t^F, & \text{for } t = 1950 \\ \log(F_{t-1}) + \varepsilon_t^F, & \text{for } 1950 < t \leq 2021 \end{cases},$$

where ε_t^F represents the inter-annual deviation in the fully selected fishing mortality rate in year t , which was assumed to follow a normal distribution with a mean of 0 and a variance of σ_F^2 . We made the assumption that the stock was near its unfished status in the initial year. Therefore, the fully selected fishing mortality rate in the initial year, denoted as F_0 , was considered negligible and fixed at 0.01.

Given the abundance of age a in year t , the annual SSB (SSB_t) was calculated as

$$SSB_t = \varphi \cdot \sum_a N_{a,t} \cdot e^{-\phi \cdot Z_{a,t}} \cdot W_a \cdot m_a,$$

where φ is the female proportion, W_a is the mean weight-at-age, m_a is the maturity-at-age (proportion of mature individuals at age a), and ϕ is the fraction of the year elapsed at the

time of spawning. Detailed information regarding the models and input values for W_a , m_a , and other parameter inputs is provided in Table 2.

Selectivity

Several factors can contribute to variations in fisheries selectivity over time, and neglecting these changes in stock assessment models can result in biased estimates of abundance and mortality rates (Gudmundsson and Gunnlaugsson, 2012). Previous studies have highlighted that assuming constant selectivity over time, when it is actually time-varying, can lead to retrospective patterns in time series quantities such as SSB and fishing mortality (Martell and Stewart, 2014; Hurtado-Ferro et al., 2015; Szuwalski et al., 2018).

As discussed by previous studies (Martell and Stewart, 2014; Hoyle et al., 2024), we considered that selectivity of the LPS fishery was time-varying and consisted of the two main components: (i) availability of fish to the fishing gear, influenced by factors such as spatial distribution of fish and variations in fishing location and effort, and (ii) retention probability of the fishing gear (i.e., the probability of capturing a fish of a given size given that the fish is available to the fishing gear).

We assumed that a time-varying component of selectivity in the LPS fishery, as indicated by the temporal changes in the left limb (i.e., small size groups) of the length composition data (see Fig. 1c), was primarily driven by changes in the availability of young fish to the fishing gear. However, we made the assumption that the retention probability of the fishing gear remained constant over time. This allowed us to model time-invariant length-at-age probability distributions in catch (see Eq. (5) in the *Length-at-age distributions in catch* section below for more details). This time-invariant assumption for length-at-age distributions was commonly made in other similarly structured models (Fournier et al., 1998; Francis, 2016).

To incorporate the time-varying component of selectivity in the LPS fishery, we developed a

model for age-dependent, time-varying selectivity, denoted $S_{a,t}$:

$$S_{a,t} = \frac{19}{19 + e^{-\log(361) \cdot \left(\frac{a-a_{95}}{a_{95}-a_{05,t}}\right)}}. \quad (1)$$

In this model, $a_{05,t}$ represents the age at which 5% selectivity occurs in year t . This value was assumed to either remain constant (i.e., the same for all years) or vary with time, depending on chosen model configurations (See the *Alternative model configurations* section below for more details). In contrast, a_{95} denotes the age at which 95% selectivity occurs, and this value was considered constant over time. Such a time-invariant assumption was made, assuming that selectivity for older age groups was relatively stable over time. This is due to the common preference in commercial fisheries for targeting large individuals. In sensitivity analyses where the constant age at 5% selectivity was assumed, we replaced $a_{05,t}$ with the median age at 5% selectivity, denoted as a_{05} .

The time-varying age at 5% selectivity was modeled using a bounded logit-normal distribution:

$$a_{05,t} = l_{a_{05}} + (u_{a_{05}} - l_{a_{05}}) \cdot \text{logit}^{-1}(x_t); \quad x_t = \text{logit} \left(\frac{a_{05} - l_{a_{05}}}{u_{a_{05}} - l_{a_{05}}} \right) + \varepsilon_t^S, \quad (2)$$

where $u_{a_{05}}$ and $l_{a_{05}}$ denote the upper and lower bounds for $a_{05,t}$, respectively, ε_t^S represents the deviation between $a_{05,t}$ and a_{05} . The vector of the deviations $\boldsymbol{\varepsilon}^S$ was assumed to follow a multivariate normal distribution with a mean vector $\mathbf{0}$ and a covariance matrix $\boldsymbol{\Sigma}$, where the covariance matrix was modeled for a stationary AR1 process with a correlation coefficient for consecutive deviations ρ :

$$\boldsymbol{\varepsilon}^S \sim \text{MVN}(\mathbf{0}, \boldsymbol{\Sigma}); \quad \boldsymbol{\Sigma}_{t,\tilde{t}} = \frac{\sigma_S^2}{1 - \rho^2} \cdot \rho^{|t-\tilde{t}|}, \quad (3)$$

where σ_S^2 is the variance of the deviation for each year t . The auto-correlation coefficient ρ was not estimated, but in sensitivity analyses was assumed to be one of 0, 0.3, 0.6, or 0.9.

Catchability

To investigate the performance of the assessment model under diverse catchability assumptions, we modeled catchability to reflect three distinct scenarios: constant, linearly increasing, and undergoing a random walk process in log space. The “linear increase” scenario was chosen to simulate the impact of technological advancements in fishing practices, such as improvements in vessel power and gear technology, as documented by Seo et al. (2017). This trend aims to capture the gradual increase in fishing efficiency over time. On the other hand, the “random walk” scenario was designed to encapsulate the potential for random fluctuations in catchability that could arise from factors not directly related to technological progress, thus providing a more comprehensive representation of variability in catchability. The catchability was modeled as follows:

$$\left\{ \begin{array}{l} q_t = q_0, \quad \text{for } 1976 \leq t \leq 2019, \\ q_t = \begin{cases} q_0, & \text{for } t = 1976 \\ q_{t-1} + c, & \text{for } 1976 < t \leq 2019 \end{cases}, \\ \log(q_t) = \begin{cases} \log(q_0), & \text{for } t = 1976 \\ \log(q_{t-1}) + \varepsilon_t^q, & \text{for } 1976 < t \leq 2019 \end{cases}, \end{array} \right. \quad \begin{array}{l} \text{if constant} \\ \text{if linear increase} \\ \text{if random walk} \end{array}, \quad (4)$$

where q_0 is either the time-invariant catchability for the “constant” assumption or the initial catchability for the “linear increase” and “random walk” assumptions, c is an additive fixed annual increase, and ε_t^q is the inter-annual deviation, which was assumed to follow a normal distribution with mean 0 and variance σ_q^2 .

Length-at-age distributions in catch

An age-length key table, based on samples collected in 2015 from the LPS fishery, is publicly available, as presented in Jung et al. (2021a). Gim et al. (2020) utilized this information to

convert length frequencies into age frequencies for all observed years of length data. They then applied an age-structured model to estimate stock status and management quantities. It is crucial to note, however, that this approach may introduce significant bias into estimates of stock size and recruitment. This potential bias arises because the age-length key table encodes the proportion of age groups within each length bin, which should be year-specific, mainly due to recruitment variability (Kimura, 1977; Westrheim and Ricker, 1978; Ailloud and Hoenig, 2019). This seemingly straightforward application overlooks the fundamental difference between the length distribution given age ($\pi_{j|a}$) and the age distribution given length ($\pi_{a|j}$) (Ailloud and Hoenig, 2019).

To address this issue, we derived the length distribution given age ($\pi_{j|a}$) using the available information on the minimum, maximum, and mean lengths of fish for each age group, as provided by Jung et al. (2021a) (see Table 2 for details). Since this information is derived from fishery catch data rather than directly from the population, we made an assumption that the length distribution follows a skew normal distribution (Azzalini, 1985), rather than a normal distribution, in order to account for selection effects in the fishery catch.

We matched the minimum, maximum, and mean lengths of fish for each age group with the 5th, 95th percentiles, and the mean of a skew normal distribution. Utilizing these matches, we derived the parameters of a skew normal distribution and applied the estimated parameters to compute the length-at-age distributions in catch, serving as input for the assessment model. The length-at-age probability distribution in catch (i.e., the probability of a fish of age a being in the j th length bin, given that it was retained in catch), denoted as $\pi_{j|a}$, was calculated as follows:

$$\pi_{j|a} = \begin{cases} \Phi(L_j + 0.5 \cdot d|\xi_a, \omega_a, \alpha_a), & \text{for } j = 1 \\ \Phi(L_j + 0.5 \cdot d|\xi_a, \omega_a, \alpha_a) - \Phi(L_j - 0.5 \cdot d|\xi_a, \omega_a, \alpha_a), & \text{for } 1 < j < J, \\ 1 - \Phi(L_j - 0.5 \cdot d|\xi_a, \omega_a, \alpha_a), & \text{for } j = J \end{cases} \quad (5)$$

where $\Phi(x|\cdot)$ is the cumulative distribution function (CDF) of the skew normal distribution for length L less than or equal to x (see Appendix B for the definition of its CDF), L_j is the midpoint of the length bin j , d is the length bin width (we set $d = 1$), and ξ_a , ω_a , and α_a are the location, scale, and shape parameters of the skew normal distribution for length-at-age a , respectively.

Observation models

The observation model components illustrate how the observed CPUE values (I_t), annual catch values (Y_t), and length composition data (\mathbf{n}_t) are linked to the age-structured population dynamics. Detailed descriptions of each observation model are provided in the following sections.

CPUE

The natural logarithm of the CPUE $\log(I_t)$ was assumed to follow a normal distribution with mean $\log(\hat{I}_t)$ and variance σ_I^2 :

$$\log(I_t) \sim \text{Normal}(\log(\hat{I}_t), \sigma_I^2),$$

where \hat{I}_t is the model-predicted CPUE in year t :

$$\hat{I}_t = q_t \cdot \text{VB}_t,$$

in which q_t is the catchability coefficient in year t , and VB_t is the biomass vulnerable to the fishery in year t . The vulnerable biomass VB_t was calculated as follows:

$$\text{VB}_t = \sum_{a=1}^A N_{a,t} \cdot e^{-0.5 \cdot Z_{a,t}} \cdot S_{a,t} \cdot W_a.$$

Annual catch

The natural logarithm of the annual catch (in weight) $\log(Y_t)$ was assumed to follow a normal distribution with mean $\log(\hat{Y}_t)$ and variance σ_Y^2 :

$$\log(Y_t) \sim \text{Normal}(\log(\hat{Y}_t), \sigma_Y^2),$$

where \hat{Y}_t is the model-predicted annual catch in year t :

$$\hat{Y}_t = \sum_{a=1}^A \hat{C}_{a,t} \cdot W_a.$$

The model-predicted age-specific catch in numbers $\hat{C}_{a,t}$ was calculated using the Baranov catch equation (Baranov, 1918):

$$\hat{C}_{a,t} = \frac{F_{a,t}}{Z_{a,t}} \cdot N_{a,t} \cdot (1 - e^{-Z_{a,t}}). \quad (6)$$

Length composition

A simulation study by Xu et al. (2020) demonstrated that a Dirichlet-multinomial (DM) distribution outperforms other commonly used data weighting methods for composition data, when time-varying selectivity is present. Thus, we employed a DM distribution to model the length composition data:

$$\mathbf{n}_t \sim \text{DM}(E_t, \boldsymbol{\delta}_t), \quad \text{for } 2000 \leq t \leq 2017,$$

where \mathbf{n}_t represents the vector of observed fish counts collected for each length bin j in year t , E_t denotes the sample size of the length composition observations in year t , and $\boldsymbol{\delta}_t$ is the vector of concentration parameters for year t (defined as how concentrated the observed length

composition proportions are around the model-predicted length composition proportions).

Following Thorson et al. (2017), we parameterized the concentration parameter for each length bin j in year t (i.e., $\delta_{j,t}$) as a function of the corresponding model-predicted length composition proportion $\hat{P}_{j|t}$ and the variance-inflation parameter β_t :

$$\delta_{j,t} = \beta_t \cdot \hat{P}_{j|t},$$

where the variance-inflation parameter β_t was assumed to have a linear relationship with both the sample size E_t and the scale parameter θ (i.e., $\beta_t = E_t \cdot \theta$). This assumption led to the formulation of the effective sample size as $E_t^{\text{eff}} = (1 + \theta \cdot E_t)/(1 + \theta)$, where E_t^{eff} represents the effective sample size for observations in year t (for further details, refer to Thorson et al. (2017)).

The model-predicted length composition proportion $\hat{P}_{j|t}$ was derived as follows:

$$\hat{P}_{j|t} = \frac{\hat{C}_{j,t}}{\sum_{j'=1}^J \hat{C}_{j',t}},$$

where $\hat{C}_{j,t}$ represents the model-predicted catch (in numbers) of fish in length bin j for year t . This catch was derived by converting the age-specific catch $\hat{C}_{a,t}$ in Eq. (6) to the length-specific catch $\hat{C}_{j,t}$, based on the length-at-age distribution in catch (i.e., $\pi_{j|a}$ in Eq. (5)):

$$\hat{C}_{j,t} = \sum_{a=1}^A \hat{C}_{a,t} \cdot \pi_{j|a}.$$

Alternative model configurations

To explore the effects of different model configurations on the model performance, we fitted a total of 15 models (denoted as M1-15) to the data, each differing in several key aspects:

- The selectivity was either constant (i.e., setting $a_{05,t} = a_{05}$ for all t in Eq. (1)) or time-varying (i.e., allowing $a_{05,t}$ in Eq (2) to vary over time).
- The auto-correlation coefficient (i.e., ρ in Eq. (3)) for deviations of age at 5% selectivity was fixed at 0.0, 0.3, 0.6, or 0.9 (note that we initially attempted to estimate ρ as part of the model fitting process, but it was found to be non-identifiable and was thus fixed at these values).
- The catchability coefficient was either constant or time-varying in two distinct ways (i.e., linearly increasing or following a random walk), as specified in Eq. (4).

Details of the model configurations are summarized in Table 3.

Standard deviation penalty function

Estimating both process and observation standard deviation (SD) parameters in state-space models is a challenging task, as highlighted in previous works (Auger-Méthé et al., 2016, 2021; Hyun and Kim, 2022; Kim, 2022). Even in a simple random walk model, these SD parameters are practically non-identifiable without additional constraints (Auger-Méthé et al., 2016). Non-identifiability of those parameters is often indicated by boundary estimates (Auger-Méthé et al., 2016, 2021; Hyun and Kim, 2022; Kim, 2022) and a flat likelihood surface near the boundary (Raue et al., 2009; Auger-Méthé et al., 2016, 2021). This non-identifiability can lead to biased estimates of the other parameters and infinite confidence intervals (Raue et al., 2009; Auger-Méthé et al., 2016, 2021; Hyun and Kim, 2022; Kim, 2022).

In our study, we aimed to simultaneously estimate both process and observation variance parameters. To accomplish this, we adopted the methodology introduced by Chung et al. (2013), applying gamma distribution penalties to the SD parameters associated with the observation models (i.e., σ_Y , σ_I , and σ_q).

The gamma distribution, serving as a penalty function for $\sigma_{X \in \{Y, I, q\}}$, was defined as follows:

$$f(\sigma_X) = \frac{\lambda^\psi}{\Gamma(\psi)} \cdot \sigma_X^{\psi-1} \cdot e^{-\lambda \cdot \sigma_X},$$

where ψ is the shape parameter and λ is the rate parameter. Chung et al. (2013) recommended setting $\psi = 2$ and $\lambda \rightarrow 0$ (to achieve this, we used an extremely small value for λ , i.e., $\lambda = 10^{-10}$). This choice of $\psi = 2$ ensures positive estimates in maximum likelihood estimation for σ_X , as the gamma distribution is zero at the origin. Furthermore, as λ approaches zero, the gamma distribution function exhibits a positive constant derivative at zero, allowing the likelihood to dominate even in the presence of strong curvature near zero (Chung et al., 2013).

The joint likelihoods of the models incorporating these gamma penalties are outlined in Table 4. We conducted a comparison between the models with and without the gamma penalties to evaluate the efficacy of this penalized estimation method.

Model estimation

The estimation process was carried out using Template Model Builder (TMB) (Kristensen et al., 2016) in R (R Core Team, 2023). The model parameters Θ were estimated by maximizing the marginal likelihood of the data $\mathcal{L}(\Theta|\mathbf{D})$ using the `nlm` optimizer in R.

In TMB, the marginal likelihood of the data $\mathcal{L}(\Theta|\mathbf{D})$ was obtained by integrating out the random effects \mathbf{Q} from the joint likelihood $\mathcal{L}(\Theta, \mathbf{Q}|\mathbf{D})$ using the Laplace approximation technique (Skaug and Fournier, 2006; Kristensen et al., 2016):

$$\mathcal{L}(\Theta|\mathbf{D}) = \int \mathcal{L}(\Theta, \mathbf{Q}|\mathbf{D}) d\mathbf{Q}.$$

Through the maximization of the marginal likelihood concerning the model parameters Θ , we obtained the estimates denoted as $\widehat{\Theta}$:

$$\widehat{\Theta} = \arg \max_{\Theta} \log[\mathcal{L}(\Theta|D)].$$

Once $\widehat{\Theta}$ was determined, TMB proceeded to estimate the random effects \mathbf{Q} by maximizing the joint likelihood with respect to \mathbf{Q} , while keeping Θ fixed at $\widehat{\Theta}$:

$$\widehat{\mathbf{Q}} = \arg \max_{\mathbf{Q}} \log[\mathcal{L}(\widehat{\Theta}, \mathbf{Q}|D)].$$

The uncertainties of the parameter estimates were assessed using the delta method, which involved calculating the determinant of the Hessian matrix of the marginal likelihood at $\widehat{\Theta}$ through numerical Cholesky decomposition (Skaug and Fournier, 2006; Kristensen et al., 2016). To determine successful model convergence, we checked if the absolute value of the maximum gradient component of the parameters was close to 0 (i.e., less than 0.1), and that the Hessian matrix was positive definite. The joint likelihoods for all models considered in this study are defined in Table 4.

Model performance evaluation

The relative performance of all alternative models was assessed using Akaike’s Information Criterion (AIC) (Akaike, 1974). AIC was calculated using the maximized marginal log-likelihoods of the models, where random effects were integrated out but the gamma distribution penalties were included, and the number of fixed-effect parameters (i.e., $AIC = -2 \cdot \log(\mathcal{L}_{MLE}) + 2 \cdot k$, where \mathcal{L}_{MLE} represents the maximized marginal log-likelihood and k is the number of fixed-effect parameters).

Previous studies have demonstrated that the marginal likelihood-based AIC is reliable for selecting the best-performing model in state-space models (Auger-Méthé et al., 2017; Miller and Hyun, 2018). To further validate the accuracy of AIC in model selection, we conducted cross-test simulations. In these simulations, we treated each candidate model as an operating

model (OM) to generate pseudo data. Subsequently, all candidate models, now serving as estimation models (EMs), were fitted to this pseudo data. We then compared the AIC values of these models to ascertain whether the matching OM and EM combination yielded the lowest AIC value. Because of the large number of candidate models in this factorial experiment, a subset of alternative models (namely M10, M11, and M12) was selected for the cross-test simulations.

Robustness of the model to observation error

Deroba et al. (2015) highlighted the common occurrence of divergence in self-tests for stock assessment models employing random walks for time-varying processes, particularly in the most recent years of the time series. They recommended conducting a self-consistency test to ensure that the model was correctly specified. In line with this recommendation, we conducted a simulation test to assess the model's robustness to observation errors.

In this simulation, we generated a pseudo dataset using the model, with parameters and random effects fixed at the estimates obtained from fitting the mackerel data. Observation errors and length frequencies were drawn randomly from the assumed distributions. Subsequently, we fitted the simulated dataset to the same model to re-estimate the parameters and random effects.

To ensure the reliability of the model, we performed 500 simulation-estimation runs for this self-consistency check. The model was considered robust if the median of the estimates from the simulation-estimation runs closely matched the true values used for simulating the pseudo dataset (Deroba et al., 2015). We visually assessed the divergence between the true and estimated values by comparing summary statistics (e.g., 2.5%, 50%, and 97.5% percentiles) of the estimated time series of key quantities of interest (e.g., total biomass, SSB, fishing mortality, and catchability) with those of the true values.

Retrospective analysis

We examined retrospective patterns to identify potential model misspecification. In integrated stock assessment models, misspecification is typically indicated by systematic changes in estimates of time series quantities when the model is fitted to data, with the sequential exclusion of the most recent data points (Hurtado-Ferro et al., 2015).

We performed a retrospective analysis by sequentially excluding the last 8 years of the data and fitting the model to the reduced dataset. To visually assess retrospective patterns, we calculated the relative difference (RD) between the estimates of time series quantities obtained from the model using the full dataset and those from the models using the reduced datasets. The RD for year t of the time series quantity ζ after removing y years of data (i.e., $\text{RD}_{t,y}(\zeta)$) was defined as follows:

$$\text{RD}_{t,y}(\zeta) = \frac{\widehat{\zeta}_{t,T-y}}{\widehat{\zeta}_{t,T}} - 1, \quad \text{for } 1950 \leq t \leq T - y,$$

where T represents the terminal year of the catch data, y indicates the number of years removed from the terminal year, which spans from 1 to g (where $g = 8$ in this study), $\widehat{\zeta}_{t,T-y}$ denotes the estimate of the quantity ζ for year t derived from the model fitted to data from 1950 to $T - y$, while $\widehat{\zeta}_{t,T}$ represents the corresponding estimate from the model fitted to the full dataset. In our retrospective analysis, we considered SSB_t and F_t as the quantities ζ .

In addition to visual inspection, we quantified the retrospective pattern using Mohn's ρ (Mohn, 1999) for the time series quantity ζ (i.e., $\rho(\zeta)$). Mohn's ρ was defined as follows:

$$\rho(\zeta) = \frac{1}{g} \sum_{y=1}^g \frac{\widehat{\zeta}_{T-y,T-y}}{\widehat{\zeta}_{T-y,T}} - 1, \quad (7)$$

where $\widehat{\zeta}_{T-y,T-y}$ represents the estimate of the quantity ζ for year $T - y$ from the model fitted to the data from 1950 to $T - y$, $\widehat{\zeta}_{T-y,T}$ is the corresponding estimate from the model fitted

to the full dataset. Given the inconsistent time series lengths for catch data (1950 to 2021), CPUE data (1976 to 2019), and length frequency data (2000 to 2017), we also computed Mohn’s ρ for the time period where all data types were available. In this case, y ranged from 4 to g , and the division by g was replaced by $g - 3$.

Establishing a definitive threshold value for Mohn’s ρ to detect retrospective patterns remains a challenge in stock assessments. Therefore, we followed the recommendations of Hurtado-Ferro et al. (2015), who proposed a practical rule of thumb for species with shorter lifespans. They suggest that Mohn’s ρ values exceeding 0.3 or falling below -0.22 can be indicative of potential retrospective patterns deserving attention.

Parametric bootstrap

To assess the bias, estimability, and uncertainty of the model parameters under each model configuration, we conducted a parametric bootstrap analysis, similar to the self-consistency test described above. However, in this analysis, the pseudo-dataset was generated from the model where the random effects were not fixed but drawn from the assumed distributions with the estimated variance parameters. Subsequently, the pseudo-dataset was fitted to the same model to re-estimate the parameters and random effects, which were then compared to the corresponding true values.

We conducted a total of 1000 simulation-estimation runs for this parametric bootstrap analysis. In each run, we checked whether the 95% confidence intervals of the estimates included the true values to investigate the 95% coverage probability of the model. The Wald method was used to compute the 95% confidence intervals of the parameters.

The bias of the parameter estimates was quantified as the median of the RD between the estimated and true values. The RD of a parameter Θ for the i th simulation-estimation run was calculated as the ratio of the estimate $\hat{\Theta}$ to the true value Θ_{true} , subtracting one:

$$\text{RD}_i(\Theta) = \frac{\hat{\Theta}_i}{\Theta_{\text{true}}} - 1 \quad (8)$$

We also assessed the estimability of the parameters by analyzing the distribution of parameter estimates obtained from the simulation-estimation runs. Inestimable parameters often exhibit multi-modal distributions, and variance parameters, especially those in state-space models, frequently display a bimodal distribution, one mode of which is near zero, as highlighted by previous studies (Auger-Méthé et al., 2016, 2021; Hyun and Kim, 2022; Kim, 2022).

Random effects validation

We evaluated the distributional assumptions of the random effects \mathbf{Q} using a simulation-based approach (Waagepetersen, 2006; Thygesen et al., 2017). To validate these assumptions, we generated 1000 sets of samples from the joint posterior distribution of \mathbf{Q} and conducted an examination.

The joint posterior distribution of \mathbf{Q} was approximated using a multivariate normal distribution. The mean vector represented the estimates of the random effects, denoted as $\widehat{\mathbf{Q}}$, and the covariance matrix was derived from the negative inverse of the Hessian matrix (Thygesen et al., 2017). The samples were then normalized using the estimated SD of the random effects, such as $\hat{\sigma}_R$, $\hat{\sigma}_F$, $\hat{\sigma}_S$, and $\hat{\sigma}_q$. For auto-correlated random effects in selectivity deviations (i.e., ϵ^S in M7-15), we multiplied the inverse of the Cholesky decomposition of the corresponding covariance matrix to normalize and decorrelate the samples.

To validate the correct specification of our model, we investigated whether the normalized samples conform to a standard normal distribution. This evaluation was conducted visually through quantile-quantile (Q-Q) plots. The challenge in interpreting these plots lies in accurately distinguishing between deviations from expected values caused by random sampling variation and actual violations of assumptions. To explore systematic deviations from a standard normal distribution, we analyzed 1000 sets of Q-Q plots. Our objective was to

establish a 95% envelope for these plots, following Rubio and Genton (2016). We visually assessed whether the 95% envelope contained the straight line with an intercept of 0 and a slope of 1, representing a perfect adherence to the normality assumption.

Results

All 15 models (M1-15) successfully converged. The initial values and parameter bounds used for each model are summarized in Supplementary Table 6. The estimates of the parameters for the length-at-age distributions in catch are given in Table 5 (see Supplementary Fig. 9 for their visualized forms). The fitted estimates compared to the observed data are presented in Supplementary Figs. 10 and 11. The estimated time-varying age at 5% selectivity and recruitment deviations are shown in Supplementary Fig. 12. Based on AIC and various model validation criteria that we used in this study (details are provided in following sections), the best-performing model was M11, characterized by time-varying selectivity with an autocorrelation coefficient $\varrho = 0.6$ and a linearly increasing catchability. Other models with identical configurations, varying only in the ϱ values, also exhibited lower AIC values when compared to the models with time-invariant selectivity (M1-3) and those with time-varying selectivity but with random walk catchability (M6, M9, M12, M15). This tendency in AIC values suggested that model selection was less sensitive to the choice of ϱ and more influenced by the choice of the catchability function combined with time-varying selectivity. The differences in terms of AIC between the best-performing model (M11) and other models are summarized in Table 3.

The cross-test for checking the accuracy of AIC in model selection revealed that AIC identified the matching model between the OM and the EM with a high rate of success for M10 (400 out of 450) and M11 (466 out of 467). However, when M12 was used as the OM, AIC failed to identify the corresponding EM (only 1 out of 354 was successful). This poor performance of AIC in model selection was attributed to the additional gamma distribution penalty term

in the likelihood function of M12, imposed on σ_q . When we removed the additional gamma distribution penalty term from M12, AIC identified the matching model with the EM even for M12 with a relatively high rate of success (306 out of 355; see Supplementary Table 7 for the detailed results). Despite the improvement, the distribution of the estimates of σ_q showed a clear bimodal pattern (Supplementary Fig. 13), indicating that the model was not well-identified. This result suggested that the additional gamma distribution penalty term was necessary for the model to be well-identified, but it also made the model selection based on AIC less reliable.

The various assumptions regarding catchability had a pronounced impact on the overall trends in fishing mortality. Models assuming constant catchability (M1, M4, M7, M10, M13) exhibited nearly monotonic decreasing trends since 1985 (see panels in the first column in Fig. 2). In contrast, models assuming linearly increasing catchability (M2, M5, M8, M11, M14) demonstrated relatively stable fishing mortality trends from 1984 until 2012, followed by abrupt increases until 2015 and subsequent decreases thereafter (see panels in the second column in Fig. 2). Models incorporating random walk catchability (M3, M6, M9, M12, M15) revealed a pattern akin to those assuming linearly increasing catchability for the last decade but with gradual increasing trends from 1980 to 2000 (see panels in the third column in Fig. 2).

The catchability trends under the random walk assumption (M3, M6, M9, M12, M15) exhibited almost monotonic increases from 1990 to 2010, followed by sudden increases from 2010 to 2015, and subsequent decreases thereafter (see panels in the third column of Fig. 3). This pattern closely resembled the fishing mortality trends observed in the same models.

The SSB trends in all models exhibit a similar pattern. They were characterized by stable fluctuations around an unfisher status from 1950 to 1970, attributed to low catch levels during this period. This was followed by a steep decrease until the early 1980s (or until 2000 in models with random walk catchability), and subsequent stability around a low SSB level

(see Fig. 4). Notably, models with constant catchability showed a slight increase during this period of low SSB, although the magnitude of the increase was not substantial (see Fig. 4). The SSB estimates from all models consistently remained below 40% of the unfished SSB (i.e., $SSB_t < 0.4 \cdot SSB_0$, where SSB_0 represents the SSB at the unfished status and serves as a proxy for interpreting the stock status in this study) for the last few decades (see Fig. 4). This indicated that, despite the implementation of the TAC-based management system for this mackerel stock since 1999 (Sim et al., 2020), the stock has not been managed sustainably.

Retrospective analysis

Systematic retrospective patterns were observed in the models with time-invariant selectivity (M1-3), as evidenced by the retrospective discrepancy measures depicted in Figs. 5 and 6. In contrast, the models with time-varying selectivity (M4-15) did not exhibit any notable retrospective patterns. This observation suggested that the introduction of time-varying selectivity effectively addressed model mis-specification.

Furthermore, the Mohn's ρ values derived from the SSB time-series of those problematic models were all negative, specifically for M1-3 (i.e., $\rho(SSB) = -0.281, -0.316, -0.29$ for M1-3, respectively). According to the guideline proposed by Hurtado-Ferro et al. (2015), where a Mohn's ρ value exceeding 0.3 or falling below -0.22 indicates the presence of retrospective patterns, these values strongly suggested the existence of significant retrospective patterns. The retrospective patterns were particularly evident during the period when three different sets of data were all available (see values in the parentheses in Figs. 5 and 6).

Although no systematic retrospective patterns were observed in the models with time-varying selectivity and random walk catchability (M6, M9, M12, M15) for the last eight years, there were indications of model mis-specification. This was evident from the systematic dome-shaped curve patterns in the SSB time-series (see Fig. 5f, i, l, and o) and the S-shaped curve patterns in the fishing mortality time-series (see Fig. 6f, i, l, and o). These systematic

patterns suggested that the models with random walk catchability were influenced by certain data points when fitted to the reduced datasets. This was further confirmed by the self-test results, where observation errors were randomized to test the robustness of the models, revealing discrepancies between the true values and the median estimates (details about the self-test results are provided in the following section).

Robustness of the model to observation error

The self-test results indicated that the models with time-invariant selectivity (M1-3) were less robust to observation errors compared to the models with time-varying selectivity (M4-15) (Figs. 2 and 3). Specifically, the true values consistently fell outside the 95% interval of the estimated values for fishing mortality and catchability time-series in most years when time-invariant selectivity was assumed (M1-3; see the panels in the first row in Figs. 2 and 3), irrespective of the catchability assumption. However, all the models, with the exception of M3, demonstrated a high level of robustness in the SSB time-series (Fig. 4; also in the total biomass time-series; see Supplementary Fig. 15). Only M3 displayed some deviation between the true values and the median estimates in the SSB time-series in the last five years (Fig. 4c).

On the contrary, the models with time-varying selectivity (M4-15) displayed a higher level of robustness against observation errors when compared to the models with time-invariant selectivity (M1-3) (Figs. 2 and 3). This improved robustness was evident through the relatively smaller discrepancies between the true values and the median estimates in the fishing mortality and catchability time-series. It is worth noting, however, that models with random walk catchability (M6, M9, M12, M15) exhibited divergent patterns in the fishing mortality and catchability time-series, especially over the last decade (see the subfigures f,i,l and o in Figs. 2 and 3). In contrast, models featuring constant catchability and linearly increasing catchability (M4, M5, M7, M8, M10, M11, M13, and M14) demonstrated greater robustness across all the considered time-series quantities (see the subfigures d, e, g, h, j, k,

m, and n in Figs. 2-4).

The convergence rates of the self-test results are summarized in Table 3. In general, the convergence rates were good, with eight models showing over 90% convergence out of 500 simulation-estimation runs. However, the models with the highest auto-correlation ($\rho = 0.9$) for selectivity deviations displayed lower convergence rates, ranging from 51% to 84%.

Bias and coverage probability of the parameter estimates

The RD measures obtained from the parametric bootstrap analysis revealed that the medians of RDs (i.e., $\text{median}[\text{RD}(\Theta)]$) were closely centered around zero, with most of them exhibiting biases within 5%, except for σ_S which showed the largest bias in all 15 models (ranging from -9.9% in M5 to -21.5% in M15; see Supplementary Fig. 14a-c). Such negative biases in process error variance parameters were commonly observed in various state-space stock assessment models (Cadigan, 2015; Miller et al., 2016; Miller and Hyun, 2018; Trijoulet et al., 2020; Kim, 2022). This phenomenon was attributed to the downward bias associated with maximum likelihood estimation (Pawitan, 2001).

Conversely, the SD parameters for the observation error (i.e., σ_Y and σ_I) exhibited slightly positive biases in the medians of the RDs, which was likely due to the gamma penalties (compare the medians of the RDs in Supplementary Fig. 14). These positive biases occurred because the estimator shifted the estimates that were close to zero to slightly larger values, thereby enhancing parameter identifiability (Chung et al., 2013) (Figs. 7 and 8). These biases ranged from 5.3% to 8.2% for models with constant catchability (M4-8) and linearly increasing catchability (M10-14), but were slightly larger for models with random walk catchability (M9, M12, M15), ranging from 10.1% to 14.3%. The biases for σ_I were small in all models, ranging from 0.1% to 6.0%. The largest bias for σ_I was observed in M6 (random walk catchability).

The convergence rates of the parametric bootstrap analysis are summarized in Table 3. Overall, the convergence rates were good, with 10 models showing over 95% convergence rates

out of 1000 simulation-estimation runs. However, the models with the highest auto-correlation ($\rho = 0.9$) for selectivity deviations displayed lower convergence rates, ranging from 80% to 86%, which aligns with the tendencies observed in the convergence rates obtained from the self-test analysis.

The 95% coverage probabilities of parameter estimates are summarized in Supplementary Table 8, where most coverage probabilities of the parameters closely aligned with the nominal level of 95%. Even those with relatively poor coverage probabilities mostly fell within the range of 90% to 98%. Notably, a_{05} exhibited poor coverage probabilities of 82%, 80%, and 81% in M13, M14, and M15, respectively, possibly attributed to the negative biases of the point estimates (Supplementary Fig. 14a-c). Similarly, the coverage probabilities for σ_Y were also suboptimal in some models (M6, M9, M12, M13, M15), showing slightly less than 90% coverage probability, possibly due to the positive biases of the point estimates. Models with constant catchability and linearly increasing catchability demonstrated consistently good coverage probabilities for all parameters. Small deviations from the nominal level may be attributed to the use of Wald intervals (i.e., $\pm 1.96 \cdot \text{SD}$ for 95% confidence intervals) for computational efficiency.

Estimability of the standard deviation parameters

In cases where gamma penalties were not applied, the distributions of $\hat{\sigma}_Y$ in all models, obtained from the parametric bootstrap analysis, exhibited bimodal shapes, with one mode near zero. This bimodality suggested that the parameter was not practically identifiable (Fig. 7). Bimodal distributions were also observed in $\hat{\sigma}_I$ in models with time-varying selectivity and random walk catchability (M6, M9, M12, and M15; see Fig. 8). When gamma penalties were applied, both $\hat{\sigma}_Y$ and $\hat{\sigma}_I$ showed unimodal distributions across all models, indicating that the parameters became identifiable regardless of the model configurations. However, the application of gamma penalties slightly shifted the distributions of $\hat{\sigma}_Y$ and $\hat{\sigma}_I$ towards the right, pushing those estimates that were close to zero towards slightly larger values (Figs. 7

and 8).

While the penalties significantly improved the estimability of σ_Y and σ_I , these enhancements did not have a substantial impact on the estimates of derived time-series quantities, such as SSB and fishing mortality (Supplementary Figs. 16 and 17). This is likely because the other random effects in the model (e.g., modeled random deviations in selectivity, recruitment, fishing mortality) had much larger impacts on the derived time-series quantities than those associated with the observation SD parameters. This phenomenon was observed in previous studies, where observation error variance parameters were not practically identifiable, but state variables and derived time-series quantities were still estimated with minimal bias (Auger-Méthé et al., 2016; Kim, 2022), especially when observation error variance parameters were smaller than process error variance parameters (Auger-Méthé et al., 2016; Kim, 2022).

Validation of the random effects assumptions

The standardized samples of random effects conformed well to the standard normal distribution across all models. This was evident from the respective Q-Q plots, where the 95% envelopes mostly covered the diagonal lines (Supplementary Figs. 18-21). However, minor systematic deviations from the diagonal lines were noted in the right tail of the median Q-Q lines for fishing mortality deviations (Supplementary Fig. 20), and in the left tail for catchability deviations (Supplementary Fig. 21). Despite these deviations, the median Q-Q lines were generally close to the diagonal lines, with the 95% envelopes largely encompassing these diagonals.

Discussion

This study demonstrated the efficacy of our proposed model in addressing unexplained temporal variability in CPUE data, without requiring additional information. Furthermore, we highlighted the capabilities of the non-degenerate estimator in handling non-identifiability

issues related to the SD parameters, thus facilitating the simultaneous estimation of all SD parameters within the model. We recommend adopting this approach in future stock assessments employing a state-space framework, especially when it is crucial to estimate both observation and process error SD parameters. However, we also acknowledge that the non-degenerate estimator introduces small bias into the estimates of SD parameters. This bias is likely to be negligible if the true SD is not too close to zero as demonstrated by Chung et al. (2013), but it is important to be aware of this bias and evaluate its potential impacts on stock assessments through simulation studies, such as the parametric bootstrap test that we conducted in this study. Furthermore, the inclusion of additional penalty terms for SD parameters in more complex models rendered AIC less effective for model selection, as demonstrated in our study. This indicates that the AIC may not be ideally suited for comparing models that incorporate differing numbers of penalty terms for SD parameters. Treating the penalty terms for SD parameters as priors can be an alternative approach to address this issue while treating SD parameters as random effects, as incorporated in WHAM (Stock and Miller, 2021), but our initial attempts to implement this approach were not successful due to convergence issues. Nonetheless, within the scope of our research, the AIC proved valuable in identifying the most effective model between those with constant and linearly increasing catchability with time-varying selectivity, since the penalty terms for SD parameters were consistent across these models. Importantly, these were the only models that met all criteria in our model checking tests.

Additionally, our findings highlighted significant enhancements achieved by incorporating time-varying selectivity and catchability into the assessment model. This integration has led to a better performing model, characterized by reduced retrospective patterns and improved goodness-of-fit. In our study, time-varying selectivity was more influential in addressing the retrospective patterns than time-varying catchability, but both components were essential in improving the model performance in terms of goodness-of-fit. The best-performing model (M11) indicated the presence of auto-correlation in the age at 5% selectivity, suggesting that

the temporal changes in the left limb of the length composition data (temporal variations in the proportion of small individuals) were partially explained by changes in selectivity, not solely by recruitment signals. However, care should be taken when interpreting this result, as we only investigated the relationship between the auto-correlation in selectivity deviations and the temporal changes in the length composition data. This relationship may be influenced by the auto-correlation in recruitment deviations, which we did not investigate in this study. We recommend that future studies explore these potential correlations to more thoroughly examine the underlying mechanisms of the temporal changes in the distribution of the length composition data. For example, a two-dimensional AR(1) process, applied in previous studies (Cadigan, 2015; Xu et al., 2019; Stock and Miller, 2021), can be used to investigate the correlation between recruitment and selectivity deviations and their auto-correlations over time.

We demonstrated that in cases where CPUE standardization is not feasible, our model-based approach provides a valuable alternative. This approach implicitly accounts for variations in CPUE without the need for supplementary data typically required by explicit CPUE standardization methods. However, it is crucial to exercise caution when implementing this approach using a random walk, as the flexibility of the random walk process may lead to overfitting and robustness issues. In our study, the random walk process for catchability was not effective in addressing the retrospective patterns, and it showed divergent patterns in the self-test (note that we refer to the self-test as the test where the observation errors were randomly generated while fixing the process errors, whereas the parametric bootstrap test refers to the test where both the observation and process errors were randomly generated). This is likely due to the fact that the random walk process was overly flexible and sensitive to the few data points influencing the overall trend. To mitigate these challenges and enhance model performance, we recommend exploring alternative formulations for the time-varying components, such as the simple linear trend that we used for time-varying catchability.

Furthermore, our self-test and parametric bootstrap results unveiled numerous potential issues with the model, encompassing biased estimates, poor convergence, and non-identifiability challenges. These simulation-based diagnostics have effectively identified misspecified models. This highlighted the importance of conducting simulation studies to thoroughly assess and ensure model performance and robustness, aligning with recommendations from previous studies (Deroba et al., 2015; Auger-Méthé et al., 2016, 2021; Kim, 2022). The full randomization of both the observation and process errors in the parametric bootstrap test was particularly useful in investigating non-identifiable parameters as well as checking uncertainty estimates through the coverage test, but this full simulation-estimation test did not indicate misspecification of the model to the observed data, as the data were simulated based on the true realizations of the process errors in each simulation run. In contrast, the self-test, where the process errors were fixed at the fitted values as the true values, and only the observation errors were randomized, was effective in identifying misspecified models, but it did not indicate issues with non-identifiability because the test was not capable of investigating the separability of the observation and process errors. Therefore, we recommend conducting both self-test and parametric bootstrap to broadly assess model performance and robustness, especially when the model is complex and the data are sparse.

In the context of stock assessment results for the mackerel stock, our study highlighted the potential for significant improvements in future assessments, particularly through the incorporation of models that consider fishery-dependent processes and the accurate utilization of the sparse age-length information. Notably, previous assessments of this stock overlooked the impacts of fishery-dependent processes on the CPUE data (Jung, 2019; Gim et al., 2020; Jung et al., 2021b; Hong et al., 2022; Gim and Hyun, 2022; Kim, 2022; Gim, 2023) and misapplied the age-length key when using age-structured models for the length frequencies (Gim et al., 2020; Gim, 2023). These simplifications and misapplications could introduce bias into assessments of stock status and fishing mortality rates, potentially leading to poor management decisions. In fact, our assessments differed from previous ones, showing more

pessimistic results. This difference occurred as some positive signals from the CPUE and length composition data were partially offset by the inclusion of time-varying catchability and selectivity. This underscores the importance of conducting thorough investigations into the potential impacts of fishery-dependent processes on key management quantities. Such examination is essential to ensure that assessment results are not unduly influenced by these processes. For example, our best model (M11), where the linear increase in catchability was included, supported the presence of vessel power creep of the LPS fishery, which was reported in the previous study (Seo et al., 2017). If future assessments are to incorporate this factor, the TAC advice may be more conservative than that from previous assessments, which did not account for the vessel power creep. Other catchability trends, such as asymptotic or exponential increases, may also be considered in future assessments, as these trends may better capture the underlying mechanisms of the catchability changes. Moreover, investigating the impact of including these time-varying components on projections may be required for future assessments and management advice, which we recommend as an area for future study.

To the best of our knowledge, this study is the first that incorporated fishery-dependent processes through time-varying catchability and selectivity into the assessment of the Korean mackerel stock, as well as conducted thorough model checking and simulation-based diagnostics to assess model performance and robustness of the results. We believe that our findings will provide valuable insights into future assessments of this stock, but we also acknowledge that our results may not represent the current status of the stock. This is because our assessment model was not developed with the most up-to-date data due to data availability and required simplifying assumptions on biological parameters, which are often necessary for data-limited assessments. For example, estimating length-at-age distributions in catch using the samples collected from the single year (i.e., year 2015) overlooks potential changes in growth of the species over time. If more data are available, a segmented approach, estimating the length-at-age distributions in distinct time blocks, can be considered to account for potential changes in growth over time. Furthermore, the selection of the DM distribution for models with

time-varying selectivity warrants additional scrutiny. Although endorsed by Xu et al. (2020), a study by Fisch et al. (2021) indicated that a logistic normal distribution outperformed the DM distribution for length composition data with large sample sizes. Despite these limitations, regarding model development and diagnostics, we believe that our study laid a solid foundation for a better understanding of the Korean mackerel stock and the development of future assessment models.

Acknowledgments

We express our gratitude to the marine science team at Dragonfly Data Science for their valuable discussions and manuscript review. Special thanks to Dr. Philipp Neubauer for his insightful comments and project management support. We also extend our appreciation to the associate editor and two anonymous reviewers for their constructive feedback and suggestions.

Author contribution statement

Kyuhan Kim: Conceptualization, Data curation, Formal analysis, Investigation, Methodology, Software, Validation, Visualization, Writing – original draft, Writing – review & editing.

Nokuthaba Sibanda: Conceptualization, Supervision, Writing - review & editing.

Richard Arnold: Conceptualization, Supervision, Writing - review & editing.

Teresa A'mar: Conceptualization, Supervision, Writing - review & editing.

Funding statement

Funding: Kyuhan Kim and Teresa A'mar were supported by the Dragonfly internal marine R&D project.

Data availability statement

Data and code to reproduce the results in this paper are available in the Zenodo repository (10.5281/zenodo.11177291, <https://doi.org/10.5281/zenodo.11177291>).

Competing interests

The authors declare there are no competing interests.

References

- Ailloud, L.E. and Hoenig, J.M. 2019. A general theory of age-length keys: combining the forward and inverse keys to estimate age composition from incomplete data. *ICES J. Mar. Sci.* **76**(6): 1515–1523. doi:<https://doi.org/10.1093/icesjms/fsz072>.
- Akaike, H. 1974. A new look at the statistical model identification. *IEEE Trans. Automat. Contr.* **19**(6): 716–723. doi:<https://doi.org/10.1109/TAC.1974.1100705>.
- Auger-Méthé, M., Field, C., Albertsen, C.M., Derocher, A.E., Lewis, M.A., Jonsen, I.D., and Mills Flemming, J. 2016. State-space models' dirty little secrets: even simple linear Gaussian models can have estimation problems. *Sci. Rep.* **6**(1): 26677. doi:<https://doi.org/10.1038/srep26677>.
- Auger-Méthé, M., Albertsen, C.M., Jonsen, I.D., Derocher, A.E., Lidgard, D.C., Studholme, K.R., Bowen, W.D., Crossin, G.T., and Flemming, J.M. 2017. Spatiotemporal modelling

- of marine movement data using Template Model Builder (TMB). *Mar. Ecol. Prog. Ser.* **565**: 237–249. doi:<https://doi.org/10.3354/meps12019>.
- Auger-Méthé, M.J., Newman, K., Cole, D., Empacher, F., Gryba, R., King, A.A., Leos-Barajas, V., Mills Flemming, J., Nielsen, A., Petris, G., and Thomas, L. 2021. A guide to state–space modeling of ecological time series. *Ecol. Monogr.* **91**(4): e01470. doi:<https://doi.org/10.1002/ecm.1470>.
- Azzalini, A. 1985. A class of distributions which includes the normal ones. *Scand. J. Stat.* pp. 171–178.
- Baranov, F. 1918. On the Question of the Biological Basis of Fisheries, volume 1. Nauchnye Issled. Ikhriologicheskii Inst. Izv.
- Cadigan, N.G. 2015. A state-space stock assessment model for northern cod, including under-reported catches and variable natural mortality rates. *Can. J. Fish. Aquat.Sci.* **73**(2): 296–308. doi:<https://doi.org/10.1139/cjfas-2015-0047>.
- Chung, Y., Rabe-Hesketh, S., Dorie, V., Gelman, A., and Liu, J. 2013. A nondegenerate penalized likelihood estimator for variance parameters in multilevel models. *Psychometrika* **78**: 685–709. doi:<https://doi.org/10.1007/s11336-013-9328-2>.
- Deroba, J.J., Butterworth, D.S., Methot Jr., R.D., De Oliveira, J.A.A., Fernandez, C., Nielsen, A., Cadrin, S.X., Dickey-Collas, M., Legault, C.M., Ianelli, J., Valero, J.L., Needle, C.L., O'Malley, J.M., Chang, Y.J., Thompson, G.G., Canales, C., Swain, D.P., Miller, D.C., Hintzen, N.T., Bertignac, M., Ibaibarriaga, L., Silva, A., Murta, A., Kell, L.T., de Moor, C.L., Parma, A.M., Dichmont, C.M., Restrepo, V.R., Ye, Y., Jardim, E., Spencer, P.D., Hanselman, D.H., Blaylock, J., Mood, M., and Hulson, P.J.F. 2015. Simulation testing the robustness of stock assessment models to error: some results from the ICES strategic initiative on stock assessment methods. *ICES J. Mar. Sci.* **72**(1): 19–30. doi:<https://doi.org/10.1093/icesjms/fst237>.

- Doubleday, W.G. 1976. A least squares approach to analysing catch at age data. ICNAF Res. Bull. **12**: 69–81.
- Fisch, N., Camp, E., Shertzer, K., and Ahrens, R. 2021. Assessing likelihoods for fitting composition data within stock assessments, with emphasis on different degrees of process and observation error. Fish. Res. **243**: 106069. doi:<https://doi.org/10.1016/j.fishres.2021.106069>.
- FishstatJ, F. 2020. FishStatJ-Software for fishery and aquaculture statistical time series. FAO Fisheries Division [online]. Rome. Updated **22**.
- Fournier, D.A., Hampton, J., and Sibert, J.R. 1998. MULTIFAN-CL: a length-based, age-structured model for fisheries stock assessment, with application to South Pacific albacore, *Thunnus alalunga*. Can. J. Fish. Aquat.Sci. **55**(9): 2105–2116. doi:<https://doi.org/10.1139/f98-100>.
- Francis, R.C. 2016. Growth in age-structured stock assessment models. Fish. Res. **180**: 77–86. doi:<https://doi.org/10.1016/j.fishres.2015.02.018>.
- Gelman, A., Vehtari, A., Simpson, D., Margossian, C.C., Carpenter, B., Yao, Y., Kennedy, L., Gabry, J., Bürkner, P.C., and Modrák, M. 2020. Bayesian workflow. arXiv:2011.01808 [stat.ME] doi:<https://doi.org/10.48550/arXiv.2011.01808>.
- Gim, J. 2019. A length-based model for Korean chub mackerel (*Scomber japonicus*) stock. Master's thesis, Pukyong National University.
- Gim, J. 2023. Assumptions about the natural mortality for a state-space age-structured assessment model: the illustration with the chub mackerel (*Scomber japonicus*) population in the Korean waters. Ph.D. thesis, Pukyong National University.
- Gim, J. and Hyun, S.Y. 2019. Importance of Considering Year-to-year Variability in Length-weight Relationship in a Size-based Fish Stock Assessment. Korean J. Fish. Aquat. Sci. **52**(6): 719–724. doi:<https://doi.org/10.5657/KFAS.2019.0719>.

- Gim, J. and Hyun, S.Y. 2022. Application of a Length-Based Stock Assessment Model for the Chub Mackerel (*Scomber japonicus*) in Korean Waters. *Ocean Sci. J.* **57**(2): 287–294. doi:<https://doi.org/10.1007/s12601-022-00067-x>.
- Gim, J., Hyun, S.Y., and Lee, J.B. 2020. Management Reference Points for Korea Chub Mackerel *Scomber japonicus* Stock. *Korean J. Fish. Aquat. Sci.* **53**(6): 942–953. doi:<https://doi.org/10.5657/KFAS.2020.0942>.
- Gudmundsson, G. and Gunnlaugsson, T. 2012. Selection and estimation of sequential catch-at-age models. *Can. J. Fish. Aquat.Sci.* **69**(11): 1760–1772. doi:<https://doi.org/10.1139/f2012-095>.
- Hilborn, R. and Walters, C.J. 1992. Quantitative fisheries stock assessment: Choice, dynamics and uncertainty. Springer Science & Business Media.
- Hilborn, R., Amoroso, R.O., Bogazzi, E., Jensen, O.P., Parma, A.M., Szuwalski, C., and Walters, C.J. 2017. When does fishing forage species affect their predators? *Fish. Res.* **191**: 211–221. doi:<https://doi.org/10.1016/j.fishres.2017.01.008>.
- Hiyama, Y., Yoda, M., and Ohshimo, S. 2002. Stock size fluctuations in chub mackerel (*Scomber japonicus*) in the East China Sea and the Japan/East Sea. *Fish. Oceanogr.* **11**(6): 347–353. doi:<https://doi.org/10.1046/j.1365-2419.2002.00217.x>.
- Hong, J.B., Kim, D.Y., and Kim, D.H. 2022. Stock Assessment of Chub Mackerel (*Scomber japonicus*) in the Northwest Pacific Ocean Based on Catch and Resilience Data. *Sustainability* **15**(1): 358. doi:<https://doi.org/10.3390/su15010358>.
- Hoyle, S.D., Campbell, R.A., Ducharme-Barth, N.D., Grüss, A., Moore, B.R., Thorson, J.T., Tremblay-Boyer, L., Winker, H., Zhou, S., and Maunder, M.N. 2024. Catch per unit effort modelling for stock assessment: A summary of good practices. *Fish. Res.* **269**: 106860. doi:<https://doi.org/10.1016/j.fishres.2023.106860>.
- Hurtado-Ferro, F., Szuwalski, C.S., Valero, J.L., Anderson, S.C., Cunningham, C.J., Johnson,

- K.F., Licandeo, R.R., McGillaird, C.R., Monnahan, C.C., Muradian, M.L., Ono, K., Vertpre, K.A., Whitten, A.R., and Punt, A.E. 2015. Looking in the rear-view mirror: bias and retrospective patterns in integrated, age-structured stock assessment models. *ICES J. Mar. Sci.* **72**(1): 99–110. doi:<https://doi.org/10.1093/icesjms/fsu198>.
- Hyun, S.Y. 2023. An Overview of the Total Allowable Catch Policy and Fish Stock Assessments in Korea. *Korean J. Fish. Aquat. Sci.* **56**(1): 1–6. doi:<https://doi.org/10.5657/KFAS.2023.0001>.
- Hyun, S.Y. and Kim, K. 2022. An evaluation of estimability of parameters in the state-space non-linear logistic production model. *Fish. Res.* **245**: 106135. doi:<https://doi.org/10.1016/j.fishres.2021.106135>.
- ICES 2023. Benchmark workshop 2 on development of msy advice using spict (wkbmsyspict2). *ICES Scientific Reports* **5**: 472. doi:<https://doi.org/10.17895/ices.pub.23372990>.
- Jung, K.M., Kim, H., and Kang, S. 2021a. A study of growth and age structure for chub mackerel, *Scomber japonicus* caught by a large purse seine in the Korean waters. *Korean J. Ichthyol.* **33**(2): 64–73. doi:<https://doi.org/10.35399/ISK.33.2.3>.
- Jung, Y. 2019. A Bayesian state-space production model for Korean chub mackerel (*Scomber japonicus*) stock. Master's thesis, Pukyong National University.
- Jung, Y., Seo, Y.I., and Hyun, S.Y. 2021b. A Bayesian state-space production model for Korean chub mackerel (*Scomber japonicus*) stock. *Fish. Aquat. Sci.* **24**(4): 139–152. doi:<https://doi.org/10.47853/FAS.2021.e14>.
- Kang, S., Jung, K.M., and Cha, H.K. 2015. First annulus formation and age determination for otoliths of chub mackerel *Scomber japonicus*. *Korean J. Fish. Aquat. Sci.* **48**(5): 760–767. doi:<https://doi.org/10.5657/KFAS.2015.0760>.
- Kim, K. 2022. State-space stock assessment models for data-moderate fisheries. Ph.D.

- thesis, Open Access Te Herenga Waka-Victoria University of Wellington. doi:<https://doi.org/10.26686/wgtn.19709488>.
- Kim, K., Hyun, S.Y., and Seo, Y.I. 2018. Inference of age compositions in a sample of fish from fish length data. *Korean J. Fish. Aquat. Sci.* **51**(1): 79–90. doi:<https://doi.org/10.5657/KFAS.2018.0079>.
- Kim, S.R., Kim, J.J., Park, H.W., Kang, S., Cha, H.K., and Baek, H.J. 2020. Maturity and spawning of the chub mackerel *Scomber japonicus* in the Korean waters. *Korean J. Fish. Aquat. Sci.* **53**(1): 9–18. doi:<https://doi.org/10.5657/KFAS.2020.0009>.
- Kimura, D.K. 1977. Statistical assessment of the age–length key. *J. Fish. Res. Board Can.* **34**(3): 317–324. doi:<https://doi.org/10.1139/f77-052>.
- Korea Fisheries Resources Agency 2023. About TAC. Korea Fisheries Resources Agency (FIRA) Website. Accessed: 2023-12-09.
- Kristensen, K., Nielsen, A., Berg, C.W., Skaug, H., and Bell, B.M. 2016. TMB: Automatic Differentiation and Laplace Approximation. *J. Stat. Softw.* **70**(5): 1–21. doi:<https://doi.org/10.18637/jss.v070.i05>.
- Lee, H.N. and Kim, H.S. 2011. Variation of fisheries conditions of mackerel (*Scomber japonicus*) fishing ground for large purse seine fisheries. *J. Korean Soc. Fish. Ocean Techno.* **47**(2): 108–117. doi:<https://doi.org/10.3796/KSFT.2011.47.2.108>.
- Martell, S. and Stewart, I. 2014. Towards defining good practices for modeling time-varying selectivity. *Fish. Res.* **158**: 84–95. doi:<https://doi.org/10.1016/j.fishres.2013.11.001>.
- Maunder, M.N. 2001. A general framework for integrating the standardization of catch per unit of effort into stock assessment models. *Can. J. Fish. Aquat.Sci.* **58**(4): 795–803. doi:<https://doi.org/10.1139/f01-029>.
- Maunder, M.N. and Langley, A.D. 2004. Integrating the standardization of catch-per-unit-of-

- effort into stock assessment models: testing a population dynamics model and using multiple data types. *Fish. Res.* **70**(2-3): 389–395. doi:<https://doi.org/10.1016/j.fishres.2004.08.015>.
- Maunder, M.N. and Punt, A.E. 2004. Standardizing catch and effort data: a review of recent approaches. *Fish. Res.* **70**(2-3): 141–159. doi:<https://doi.org/10.1016/j.fishres.2004.08.002>.
- Maunder, M.N., Sibert, J.R., Fonteneau, A., Hampton, J., Kleiber, P., and Harley, S.J. 2006. Interpreting catch per unit effort data to assess the status of individual stocks and communities. *ICES J. Mar. Sci.* **63**(8): 1373–1385. doi:<https://doi.org/10.1016/j.icesjms.2006.05.008>.
- Miller, T.J. and Hyun, S.Y. 2018. Evaluating evidence for alternative natural mortality and process error assumptions using a state-space, age-structured assessment model. *Can. J. Fish. Aquat.Sci.* **75**(5): 691–703. doi:<https://doi.org/10.1139/cjfas-2017-0035>.
- Miller, T.J., Hare, J.A., and Alade, L.A. 2016. A state-space approach to incorporating environmental effects on recruitment in an age-structured assessment model with an application to southern new england yellowtail flounder. *Can. J. Fish. Aquat.Sci.* **73**(8): 1261–1270. doi:<https://doi.org/10.1139/cjfas-2015-0339>.
- Mohn, R. 1999. The retrospective problem in sequential population analysis: An investigation using cod fishery and simulated data. *ICES J. Mar. Sci.* **56**(4): 473–488. doi:<https://doi.org/10.1006/jmsc.1999.0481>.
- Nielsen, A. and Berg, C.W. 2014. Estimation of time-varying selectivity in stock assessments using state-space models. *Fish. Res.* **158**: 96–101. doi:<https://doi.org/10.1016/j.fishres.2014.01.014>.
- Nishijima, S., Kamimura, Y., Yukami, R., Manabe, A., Oshima, K., and Ichinokawa, M. 2021. Update on natural mortality estimators for chub mackerel in the Northwest Pacific Ocean. Technical report, NPFC-2021-TWG CMSA04-WP05.
- Ono, K., Punt, A.E., and Rivot, E. 2012. Model performance analysis for Bayesian biomass

- dynamics models using bias, precision and reliability metrics. *Fish. Res.* **125**: 173–183. doi:<https://doi.org/10.1016/j.fishres.2012.02.022>.
- Parent, E. and Rivot, E. 2012. Introduction to hierarchical Bayesian modeling for ecological data. Chapman and Hall/CRC. doi:<https://doi.org/10.1201/b12501>.
- Pawitan, Y. 2001. In all likelihood: statistical modelling and inference using likelihood. Oxford University Press.
- Pedersen, M.W. and Berg, C.W. 2017. A stochastic surplus production model in continuous time. *Fish Fish.* **18**(2): 226–243. doi:<https://doi.org/10.1111/faf.12174>.
- Punt, A.E. 2023. Those who fail to learn from history are condemned to repeat it: A perspective on current stock assessment good practices and the consequences of not following them. *Fish. Res.* **261**: 106642. doi:<https://doi.org/10.1016/j.fishres.2023.106642>.
- Punt, A.E., Hurtado-Ferro, F., and Whitten, A.R. 2014. Model selection for selectivity in fisheries stock assessments. *Fish. Res.* **158**: 124–134. doi:<https://doi.org/10.1016/j.fishres.2013.06.003>.
- R Core Team 2023. R: A Language and Environment for Statistical Computing. R Foundation for Statistical Computing, Vienna, Austria.
- Rankin, P.S. and Lemos, R.T. 2015. An alternative surplus production model. *Ecol. Modell.* **313**: 109–126. doi:<https://doi.org/10.1016/j.ecolmodel.2015.06.024>.
- Raue, A., Kreutz, C., Maiwald, T., Bachmann, J., Schilling, M., Klingmüller, U., and Timmer, J. 2009. Structural and practical identifiability analysis of partially observed dynamical models by exploiting the profile likelihood. *Bioinformatics* **25**(15): 1923–1929. doi:<https://doi.org/10.1093/bioinformatics/btp358>.
- Rohatgi, A. 2022. Webplotdigitizer: Version 4.6.
- Rubio, F.J. and Genton, M.G. 2016. Bayesian linear regression with skew-symmetric error

- distributions with applications to survival analysis. *Stat. Med.* **35**(14): 2441–2454. doi:
<https://doi.org/10.1002/sim.6897>.
- Seo, Y.I., Hwang, K.S., Cha, H.K., Oh, T.Y., Jo, H.S., Kim, B.Y., Ryu, K.J., and Lee, Y.W. 2017. Change of relative fishing power index from technological development in the offshore large powered purse seine fishery. *J. Korean Soc. Fish. Ocean Techno.* **53**(1): 12–18. doi:<https://doi.org/10.3796/KSFT.2017.53.1.012>.
- Sim, S., Lee, J., and Oh, S. 2020. An analysis of the effects in the TAC system by analyzing catch of TAC target species. *Ocean Polar Res.* **42**(2): 157–169. doi:<https://doi.org/10.4217/OPR.2020.42.2.157>.
- Skaug, H.J. and Fournier, D.A. 2006. Automatic approximation of the marginal likelihood in non-Gaussian hierarchical models. *Comput. Stat. Data Anal.* **51**(2): 699–709. doi:
<https://doi.org/10.1016/j.csda.2006.03.005>.
- Stock, B.C. and Miller, T.J. 2021. The Woods Hole Assessment Model (WHAM): a general state-space assessment framework that incorporates time-and age-varying processes via random effects and links to environmental covariates. *Fish. Res.* **240**: 105967. doi:
<https://doi.org/10.1016/j.fishres.2021.105967>.
- Szuwalski, C.S., Vert-Pre, K.A., Punt, A.E., Branch, T.A., and Hilborn, R. 2015. Examining common assumptions about recruitment: a meta-analysis of recruitment dynamics for worldwide marine fisheries. *Fish Fish.* **16**(4): 633–648. doi:<https://doi.org/10.1111/faf.12083>.
- Szuwalski, C.S., Ianelli, J.N., and Punt, A.E. 2018. Reducing retrospective patterns in stock assessment and impacts on management performance. *ICES J. Mar. Sci.* **75**(2): 596–609. doi:<https://doi.org/10.1093/icesjms/fsx159>.
- Thorson, J.T. and Minto, C. 2015. Mixed effects: a unifying framework for statistical

- modelling in fisheries biology. *ICES J. Mar. Sci.* **72**(5): 1245–1256. doi:<https://doi.org/10.1093/icesjms/fsu213>.
- Thorson, J.T., Johnson, K.F., Methot, R.D., and Taylor, I.G. 2017. Model-based estimates of effective sample size in stock assessment models using the Dirichlet-multinomial distribution. *Fish. Res.* **192**: 84–93. doi:<https://doi.org/10.1016/j.fishres.2016.06.005>.
- Thygesen, U.H., Albertsen, C.M., Berg, C.W., Kristensen, K., and Nielsen, A. 2017. Validation of ecological state space models using the Laplace approximation. *Environ. Ecol. Stat.* **24**: 317–339. doi:<https://doi.org/10.1007/s10651-017-0372-4>.
- Trijoulet, V., Fay, G., and Miller, T.J. 2020. Performance of a state-space multispecies model: What are the consequences of ignoring predation and process errors in stock assessments? *J. Appl. Ecol* **57**(1): 121–135. doi:<https://doi.org/10.1111/1365-2664.13515>.
- Waagepetersen, R. 2006. A simulation-based goodness-of-fit test for random effects in generalized linear mixed models. *Scand. J. Stat.* **33**(4): 721–731. doi:<https://doi.org/10.1111/j.1467-9469.2006.00504.x>.
- Westrheim, S. and Ricker, W. 1978. Bias in using an age–length key to estimate age-frequency distributions. *J. Fish. Res. Board Can.* **35**(2): 184–189. doi:<https://doi.org/10.1139/f78-03>.
- Wilberg, M.J. and Bence, J.R. 2006. Performance of time-varying catchability estimators in statistical catch-at-age analysis. *Can. J. Fish. Aquat.Sci.* **63**(10): 2275–2285. doi:<https://doi.org/10.1139/f06-111>.
- Wilberg, M.J., Thorson, J.T., Linton, B.C., and Berkson, J. 2009. Incorporating time-varying catchability into population dynamic stock assessment models. *Reviews fish. sci.* **18**(1): 7–24. doi:<https://doi.org/10.1080/10641260903294647>.
- Xu, H., Thorson, J.T., Methot, R.D., and Taylor, I.G. 2019. A new semi-parametric method for autocorrelated age-and time-varying selectivity in age-structured assessment models. *Can. J. Fish. Aquat.Sci.* **76**(2): 268–285. doi:<https://doi.org/10.1139/cjfas-2017-0446>.

Xu, H., Thorson, J.T., and Methot, R.D. 2020. Comparing the performance of three data-weighting methods when allowing for time-varying selectivity. *Can. J. Fish. Aquat.Sci.* **77**(2): 247–263. doi:<https://doi.org/10.1139/cjfas-2019-0107>.

Table 1. Definition of terms used in this study

Notation	Description
t, a, j	Indices for year, age, and length bin, respectively
\bar{R}	Average recruitment
ε_t^R	Inter-annual deviations in natural logarithm of average recruitment
A	Terminal age class
M	Instantaneous rate of natural mortality
$N_{a,t}$	Abundance by age and year
$\hat{C}_{a,t}$	Predicted catch by age and year
$\hat{C}_{j,t}$	Predicted catch by length group and year
$S_{a,t}$	Fishery selectivity by age and year
$Z_{a,t}$	Instantaneous rate of total mortality by age and year
$F_{a,t}$	Instantaneous rate of fishing mortality by age and year
F_0	Average instantaneous rate of fully selected fishing mortality for a pre-data period
F_t	Instantaneous rate of fully selected fishing mortality by year
ε_t^F	Inter-annual deviations in natural logarithm of fishing mortality
σ_F^2	Variance of inter-annual deviations in natural logarithm of fishing mortality
a_{95}	Age at 95% selectivity
a_{05}	Age at 5% selectivity used as a constant or median value for a time-varying model
l_Θ, u_Θ	Lower and upper bounds for a bounded logit transformation of a parameter Θ
$a_{05,t}$	Time-varying age at 5% selectivity
ε_t^S	Inter-annual deviations in logit-transformed age at 5% selectivity
$\boldsymbol{\varepsilon}^S$	Vector of inter-annual deviations in logit-transformed age at 5% selectivity
σ_S^2	Variance of inter-annual deviations in logit-transformed age at 5% selectivity
ρ	Autocorrelation coefficient for ε_t^S in a stationary AR(1) process
q_0	Catchability coefficient used as a constant or initial value for a time-varying model
q_t	Time-varying catchability coefficient
c	Additive constant for the linear increase in catchability
ε_t^q	Inter-annual deviations in catchability
σ_q^2	Variance of inter-annual deviations in catchability
$\pi_{j a}$	Probability of fish of age a being in length group j
$\Phi(\cdot)$	Cumulative distribution function of a skew normal distribution
$\xi_a, \omega_a, \alpha_a$	Location, scale, and shape parameters of a skew normal distribution
I_t, \hat{I}_t	Observed and predicted catch-per-unit-effort (CPUE), respectively
σ_I^2	Variance of observation errors in CPUE
VB_t	Vulnerable biomass by year
W_a	Mean weight-at-age
L_a	Mean length-at-age
SSB_t	Spawning stock biomass by year
m_a	Mean maturity-at-age
ϕ	Fraction of a year elapsed when spawning
φ	Female proportion in a population
Y_t, \hat{Y}_t	Observed and predicted catch (in weight) by year, respectively
σ_Y^2	Variance of observation errors in catch (in weight)
\mathbf{n}_t	Vector of observed length frequencies by year
E_t	Sample size of observed length frequencies by year
δ_t	Concentration parameters of the Dirichlet-multinomial distribution
$\hat{\mathbf{P}}_t$	Vector of predicted length proportions by year
$\hat{P}_{j t}$	Predicted proportion of fish in length group j by year
E_t^{eff}	Effective sample size of observed length frequencies by year
θ	Scale parameter in the Dirichlet-multinomial (DM) distribution
$\delta_{j,t}, \beta_t$	Concentration and variance-inflation parameters in the DM distribution, respectively
$\Theta, \mathbf{Q}, \mathbf{D}$	Vector of all parameters, random effects, and data, respectively
ψ, λ	Shape and rate parameters of the gamma distribution, respectively

Table 2. Description of quantities and sub-models with corresponding parameter values and references. The minimum, maximum, and mean lengths were utilized in estimating the length-at-age distributions in catch using skew normal distributions. In cases where the column is left blank under the "Reference" heading, it denotes that the value was not obtained from a published source and instead chosen based on the best guess of the authors of this study.

Description (notation)	Quantity or Equation	Reference
Quantity		
Minimum length-at-age	19.1, 23.1, 26.1, 30.1, 31.1, 35.1 (cm)	Jung et al. (2021a)
Maximum length-at-age	29.0, 33.0, 36.0, 42.0, 43.0, 44.0 (cm)	Jung et al. (2021a)
Mean length-at-age (L_a)	23.9, 27.8, 30.6, 34.8, 37.2, 40.1 (cm)	Jung et al. (2021a)
Natural mortality (M)	0.53 (year ⁻¹)	Nishijima et al. (2021)
Year elapsed when spawning (ϕ)	0.5 (fraction of the year)	Kim et al. (2020)
Female proportion (φ)	0.5	
Pre-data fishing mortality (F_0)	0.01 (year ⁻¹)	
Model		
Mean weight-at-age (W_a)	$W_a = 0.003 \cdot 10^{-6} \cdot L_a^{3.425}$ (MT)	Gim and Hyun (2019)
Mean maturity-at-age (m_a)	$m_a = 1/[1 + \exp(20.11 - 0.7 \cdot L_a)]$	Kim et al. (2020)

Table 3. Configuration of all 15 models fitted to the mackerel data, based on various assumptions concerning catchability (q_t), selectivity ($a_{05,t}$), and autocorrelation (ρ) of the selectivity deviation. ΔAIC represents the difference in AIC compared to the best model (M11). Convergence rates denote the percentage of successful convergence out of 500 for self-tests with randomized observation errors (Self-obs) and 1000 for self-tests with both randomized observation and process errors (Self-both; parametric bootstrap).

Model	Assumption			ΔAIC	Convergence rate (%)	
	q_t	$a_{05,t}$	ρ		Self-obs	Self-both
M1	Constant	Constant	—	112.914	89	97
M2	Linear increase	Constant	—	101.948	94	95
M3	Random walk	Constant	—	197.440	79	96
M4	Constant	Random	0.0	30.656	96	92
M5	Linear increase	Random	0.0	6.488	96	96
M6	Random walk	Random	0.0	99.117	95	86
M7	Constant	Random	0.3	26.209	90	96
M8	Linear increase	Random	0.3	1.920	96	96
M9	Random walk	Random	0.3	93.658	86	95
M10	Constant	Random	0.6	24.904	91	95
M11	Linear increase	Random	0.6	0.000	95	96
M12	Random walk	Random	0.6	90.512	84	95
M13	Constant	Random	0.9	25.508	51	86
M14	Linear increase	Random	0.9	2.683	84	80
M15	Random walk	Random	0.9	92.585	67	80

Table 4. Equations for the joint likelihood of all alternative models (M1-15) when fitted, along with components of the likelihood for observation error and process error. Gamma distributions were applied as penalty functions for three standard deviation parameters (σ_I , σ_Y , and σ_q). Note that the gamma distribution here is parameterized by the shape and rate (i.e., the reciprocal of the scale parameter) parameters.

Description	Equation
Likelihood (process error)	
Recruitment deviation	$\mathcal{L}_R = \prod_{t=1950}^{2021} \text{Normal}(\varepsilon_t^R 0, \sigma_R^2)$
Fishing mortality deviation	$\mathcal{L}_F = \prod_{t=1950}^{2021} \text{Normal}(\varepsilon_t^F 0, \sigma_F^2)$
Catchability deviation	$\mathcal{L}_q = \prod_{t=1977}^{2019} \text{Normal}(\varepsilon_t^q 0, \sigma_q^2)$
Selectivity deviation	$\mathcal{L}_S = \text{MVN}(\boldsymbol{\varepsilon}^S \mathbf{0}, \boldsymbol{\Sigma})$
Likelihood (observation error)	
CPUE	$\mathcal{L}_I = \prod_{t=1976}^{2019} \text{Normal}(\log(I_t) \log(\hat{I}_t), \sigma_I^2)$
Catch	$\mathcal{L}_Y = \prod_{t=1950}^{2017} \text{Normal}(\log(Y_t) \log(\hat{Y}_t), \sigma_Y^2)$
Length frequency	$\mathcal{L}_{LF} = \prod_{t=2000}^{2017} \text{DM}(\mathbf{n}_t E_t, \boldsymbol{\delta}_t)$
Gamma distribution penalties	
CPUE error	$f_I = \text{Gamma}(\sigma_I 2, 10^{-10})$
Catch error	$f_Y = \text{Gamma}(\sigma_Y 2, 10^{-10})$
Catchability deviation	$f_q = \text{Gamma}(\sigma_q 2, 10^{-10})$
Joint likelihood for each model	
M1, M2	$\mathcal{L}(\boldsymbol{\Theta}, \mathbf{Q} \mathbf{D}) = \mathcal{L}_R \cdot \mathcal{L}_F \cdot \mathcal{L}_{LF} \cdot \mathcal{L}_I \cdot \mathcal{L}_Y \cdot f_I \cdot f_Y$
M3	$\mathcal{L}(\boldsymbol{\Theta}, \mathbf{Q} \mathbf{D}) = \mathcal{L}_R \cdot \mathcal{L}_F \cdot \mathcal{L}_q \cdot \mathcal{L}_{LF} \cdot \mathcal{L}_I \cdot \mathcal{L}_Y \cdot f_I \cdot f_Y \cdot f_q$
M4, M5, M7, M8, M10, M11, M13, M14	$\mathcal{L}(\boldsymbol{\Theta}, \mathbf{Q} \mathbf{D}) = \mathcal{L}_R \cdot \mathcal{L}_F \cdot \mathcal{L}_S \cdot \mathcal{L}_{LF} \cdot \mathcal{L}_I \cdot \mathcal{L}_Y \cdot f_I \cdot f_Y$
M6, M9, M12, M15	$\mathcal{L}(\boldsymbol{\Theta}, \mathbf{Q} \mathbf{D}) = \mathcal{L}_R \cdot \mathcal{L}_F \cdot \mathcal{L}_q \cdot \mathcal{L}_S \cdot \mathcal{L}_{LF} \cdot \mathcal{L}_I \cdot \mathcal{L}_Y \cdot f_I \cdot f_Y \cdot f_q$

Table 5. Estimates of the parameters for the skew normal distribution representing length-at-age distributions in catch. ξ_a , ω_a , and α_a are the location, scale, and shape parameters for the skew normal distribution for age a , respectively.

Parameter	Age (a)					
	0	1	2	3	4	5
ξ_a	21.691	25.200	27.471	29.911	39.702	43.199
ω_a	3.735	3.980	4.352	6.168	4.400	4.132
α_a	1.104	1.425	2.080	8.687	-1.016	-2.752

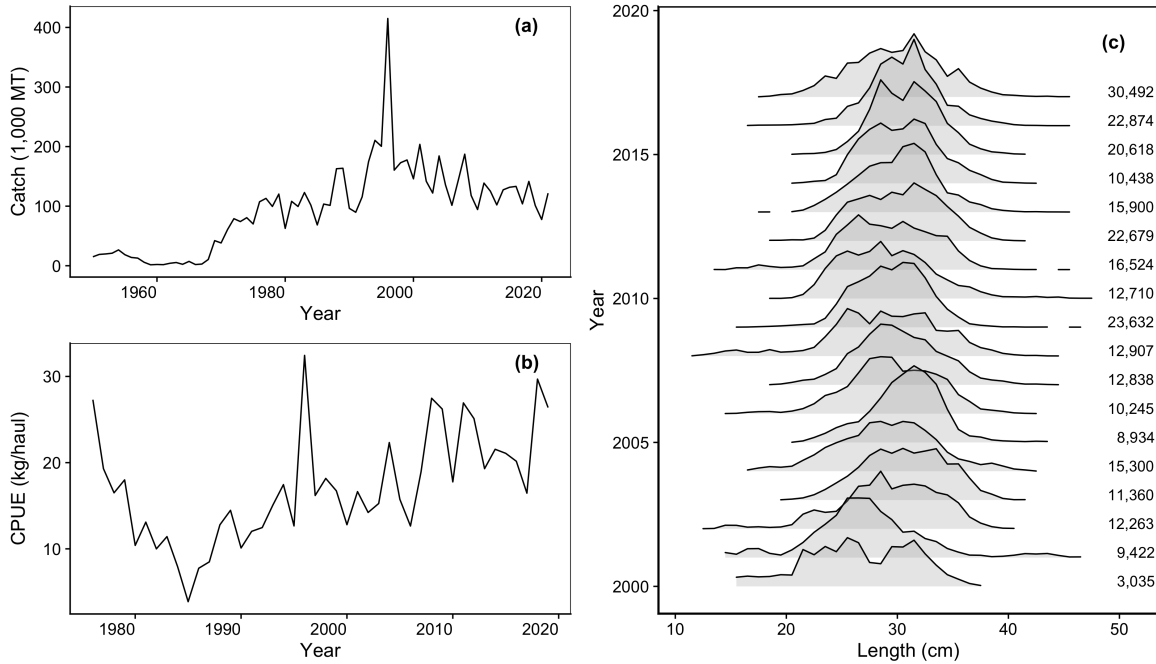


Fig. 1. Catch (a), catch-per-unit-effort (CPUE) (b), and length composition (c) data from the mackerel stock. The CPUE and length composition data were collected from the large purse seine fishery only. The length composition data are shown as the proportion of fish in each length bin. The numbers in the panel (c) indicate sample sizes for each year.

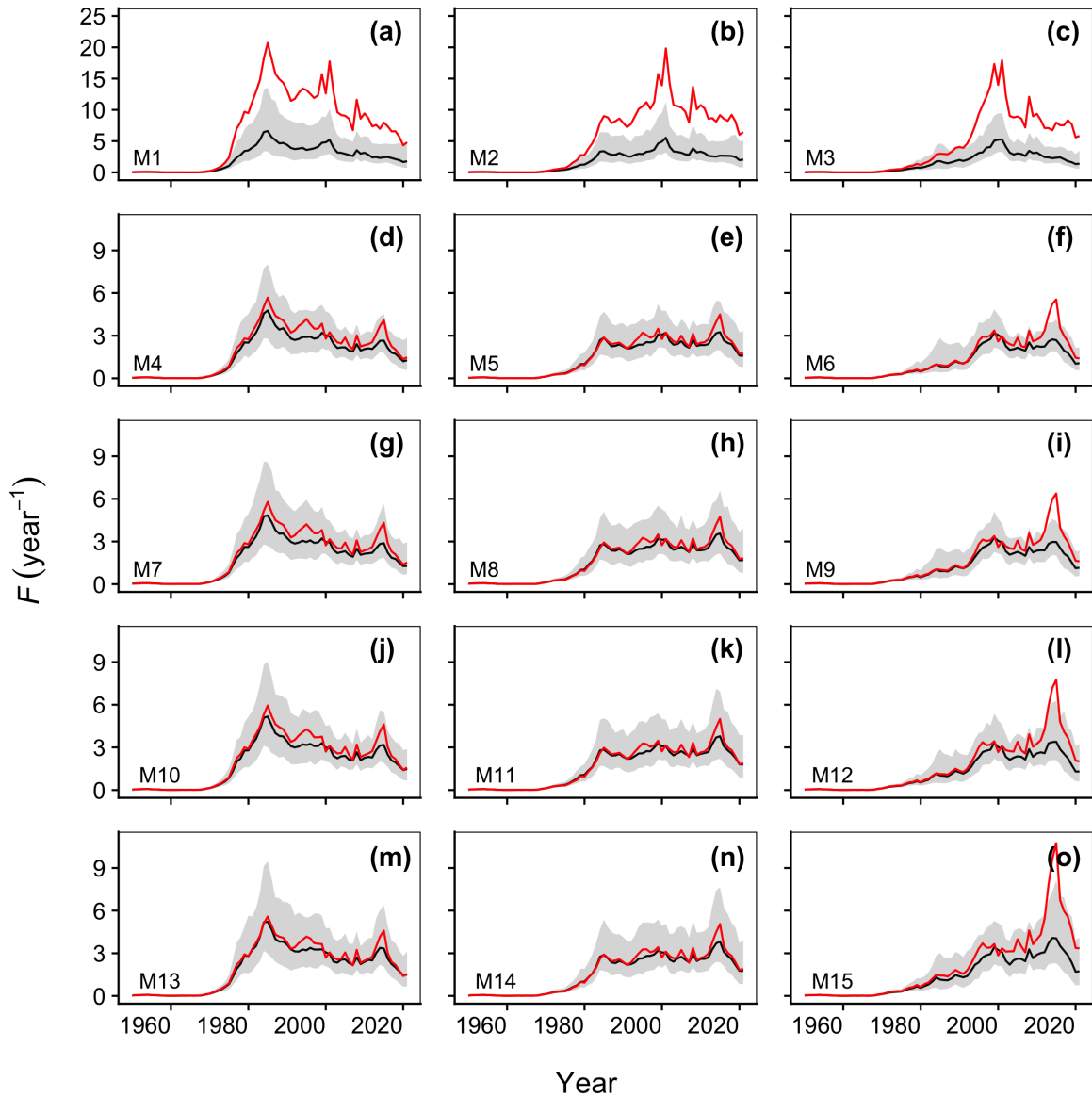


Fig. 2. Self-test estimates of the fishing mortality rate (F) and corresponding true values for all alternative models (M1-15), with the name of the corresponding model denoted at the bottom left corner of each panel. The black lines indicate the median values of the self-test estimates, and the gray areas indicate the 95% intervals. The red lines indicate the true values.

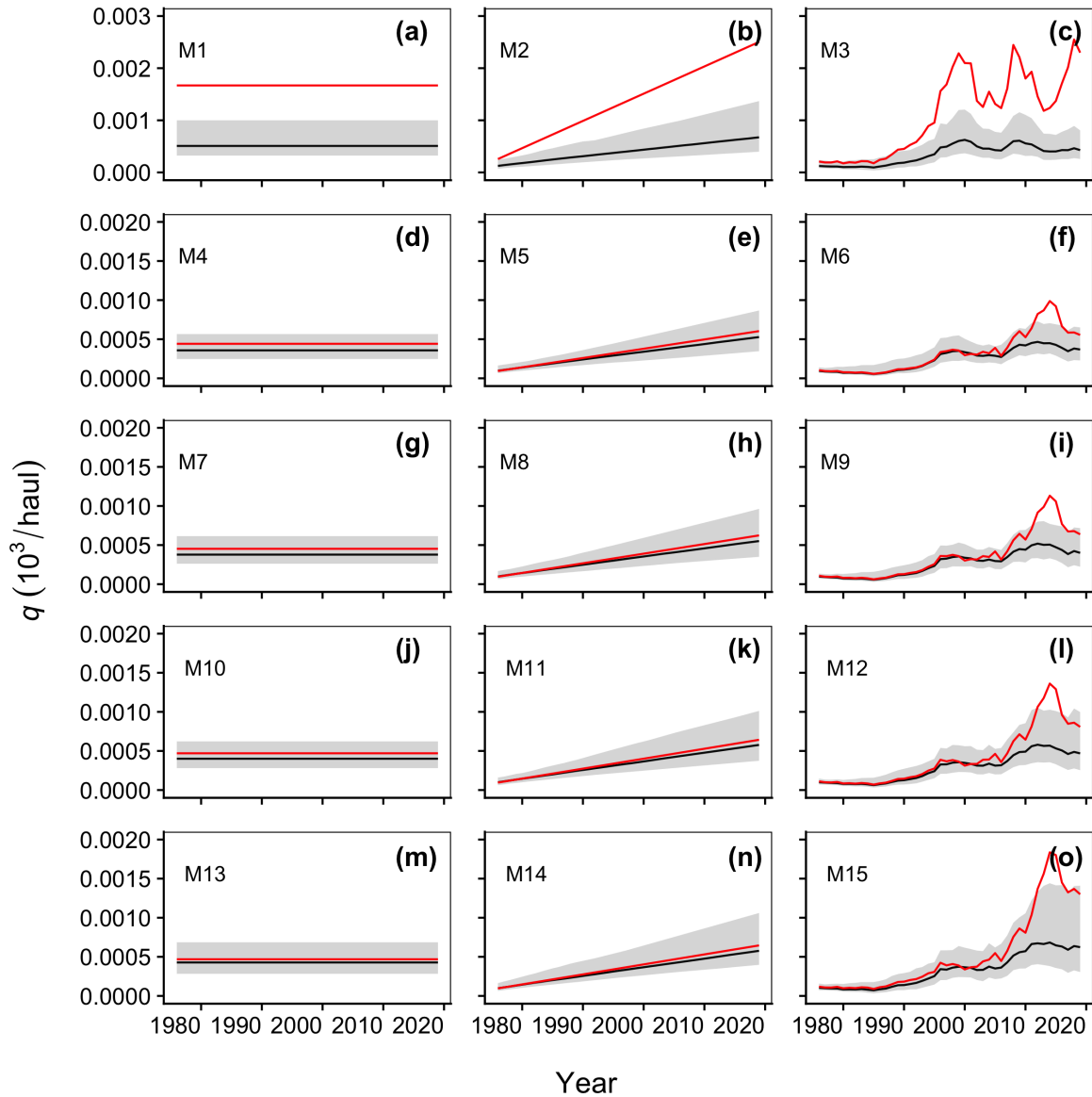


Fig. 3. Self-test estimates of the catchability (q) and corresponding true values for all alternative models (M1-15), with the name of the corresponding model denoted at the top left corner of each panel. The black lines indicate the median values of the self-test estimates, and the gray areas indicate the 95% intervals. The red lines indicate the true values.

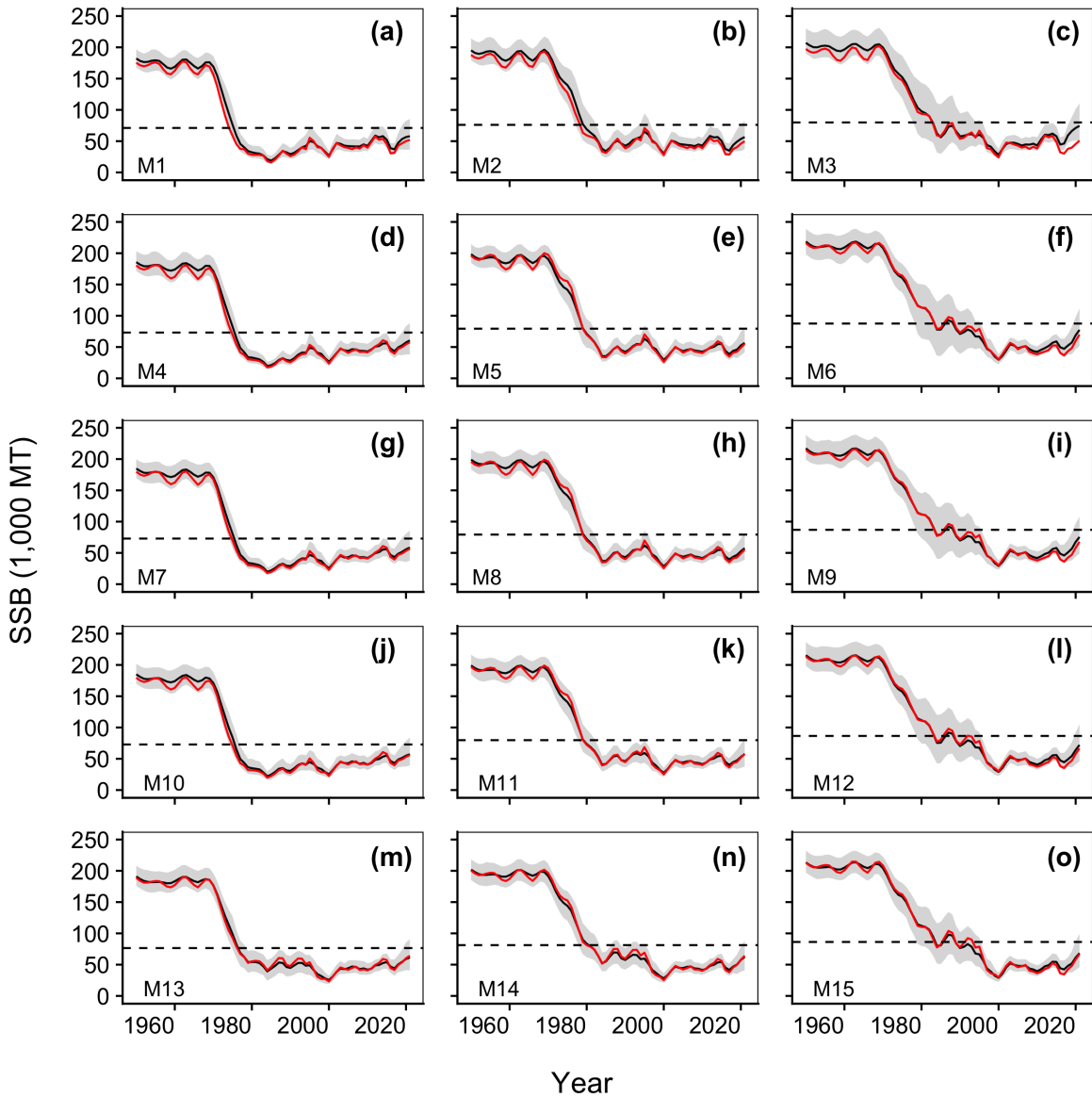


Fig. 4. Self-test estimates of the spawning stock biomass (SSB) and corresponding true values for all alternative models (M1-15), with the model name indicated in the bottom-left corner of each panel. The black lines indicate the median values of the self-test estimates, and the gray areas represent the 95% intervals. The red lines indicate the true values. The horizontal dashed lines denote the 40% of the virgin spawning stock biomass level for each model.

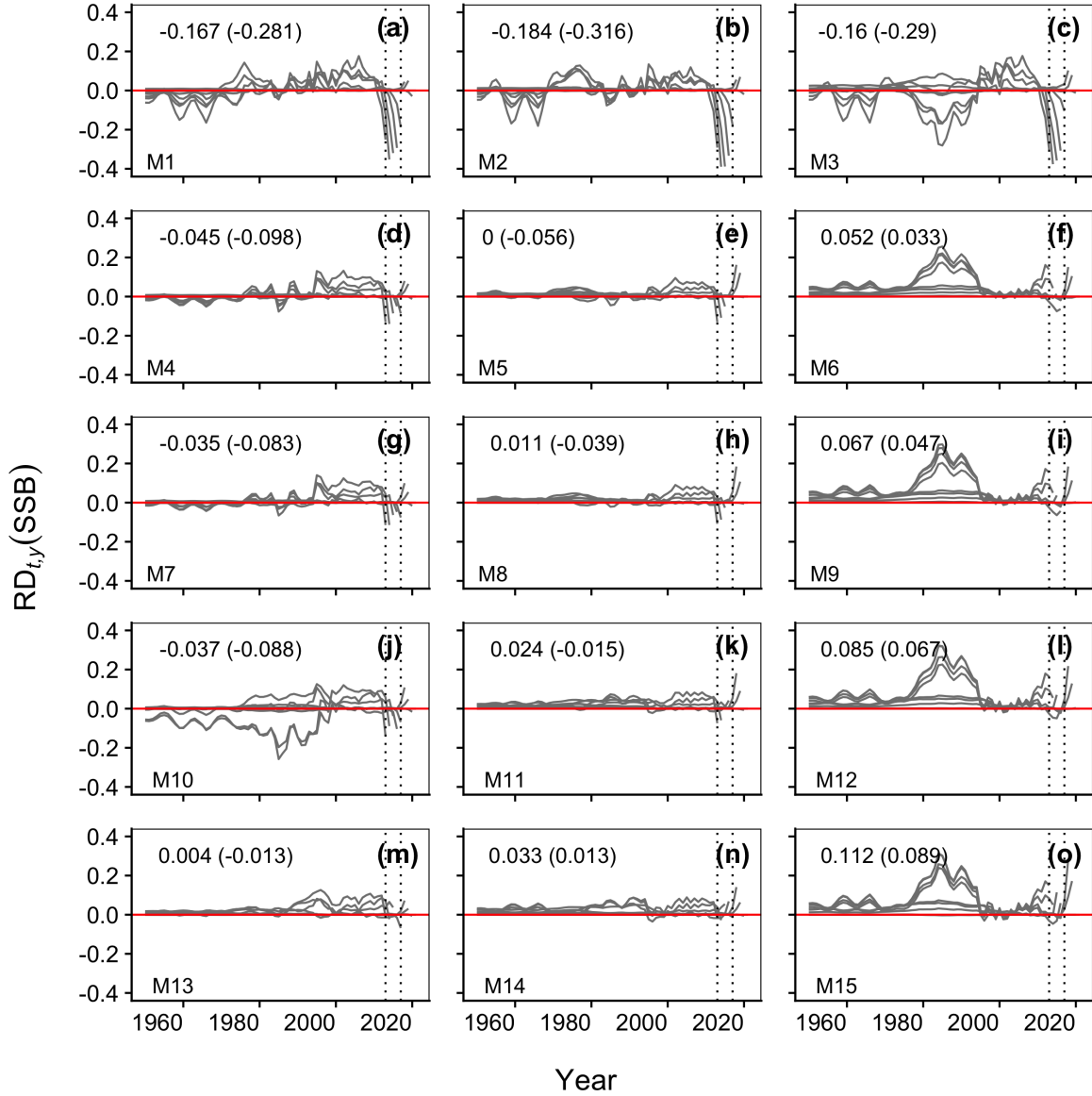


Fig. 5. Relative difference (RD) measures (gray lines) for visualizing retrospective patterns in the estimated spawning stock biomass (SSB) for all alternative models (M1-15), with the model name indicated in the bottom-left corner of each panel. RD was calculated as the difference between estimates from the model fitted to the full dataset and the model fitted to the iteratively removed data for the last eight years, divided by the estimates from the model fitted to the full dataset. The horizontal red line indicates no difference between the two estimates, and the two vertical dotted lines mark the time period when all three datasets were available when fitting the model to the reduced dataset. The values at the top left corner of each panel indicate Mohn's ρ values for all eight years of iterative data removal and fitting, with values in parentheses indicating the ρ values for the five years of iterative data removal and fitting (2013 to 2017), a period during which complete data was available (between the two vertical dotted lines).

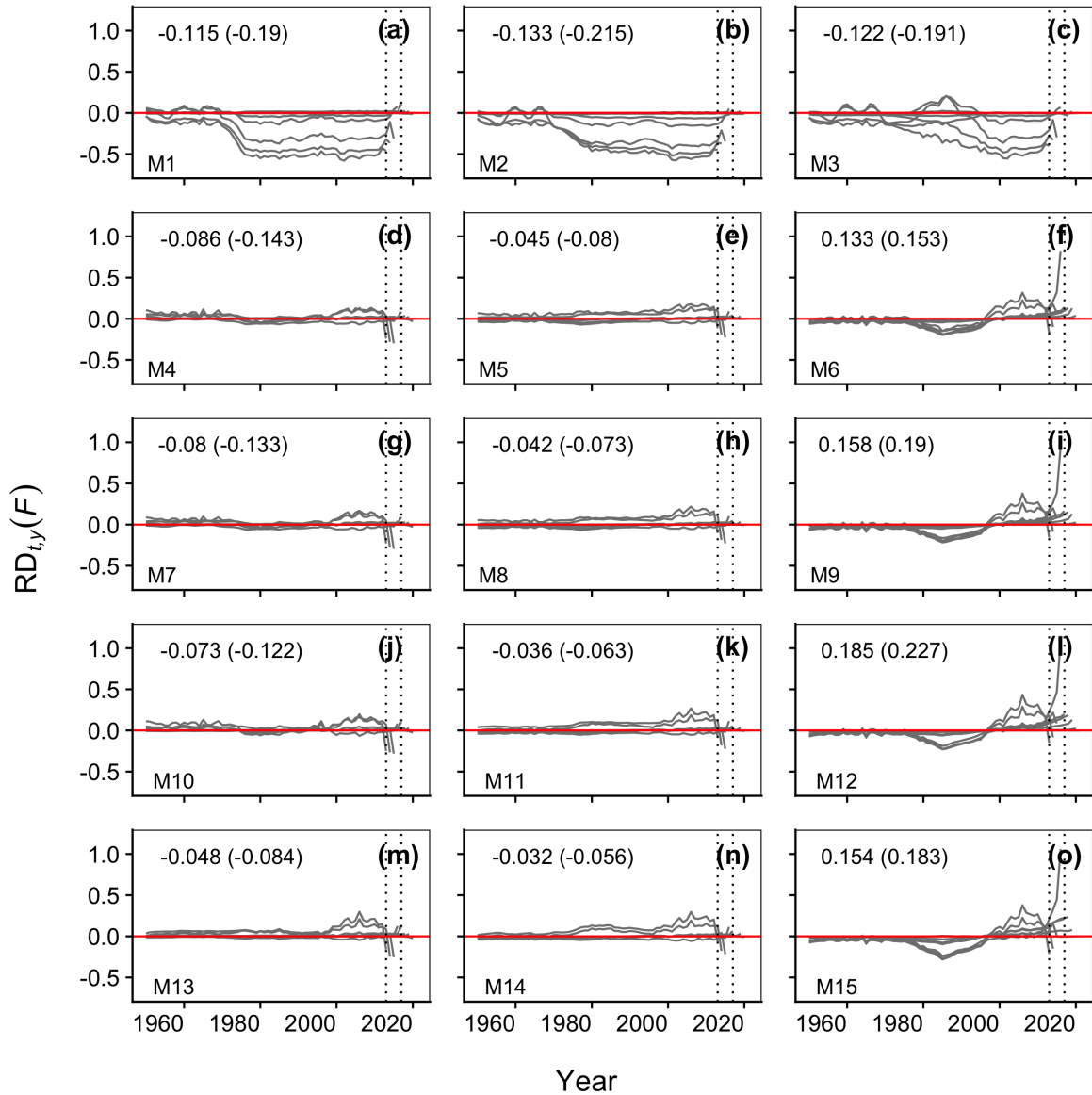
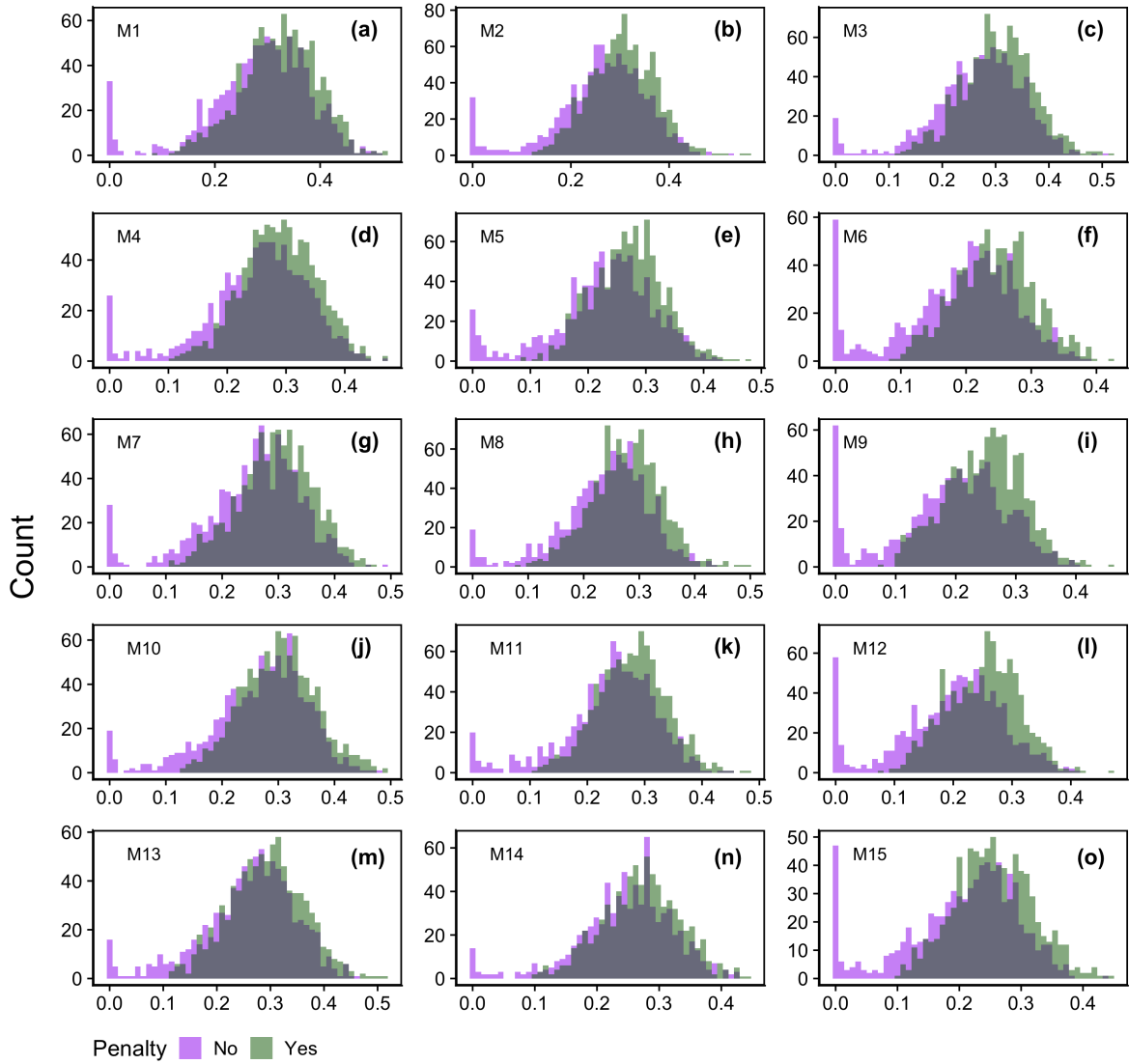


Fig. 6. Relative difference (RD) measures (gray lines) for visualizing retrospective patterns in the estimated fishing mortality rate (F) for all alternative models (M1-15), with the model name indicated in the bottom-left corner of each panel. Other details about the calculation of RD are as described in Fig. 5.



$$\hat{\sigma}_Y$$

Fig. 7. Histograms of the estimates of the standard deviation parameter for the observation error of the annual catch ($\hat{\sigma}_Y$), with (dark green) and without (purple) the gamma penalty on the parameter. Each panel displays histograms of the parameter estimated from a different model, with the model name indicated in the top-left corner. The estimates were obtained from the parametric bootstrap analysis.

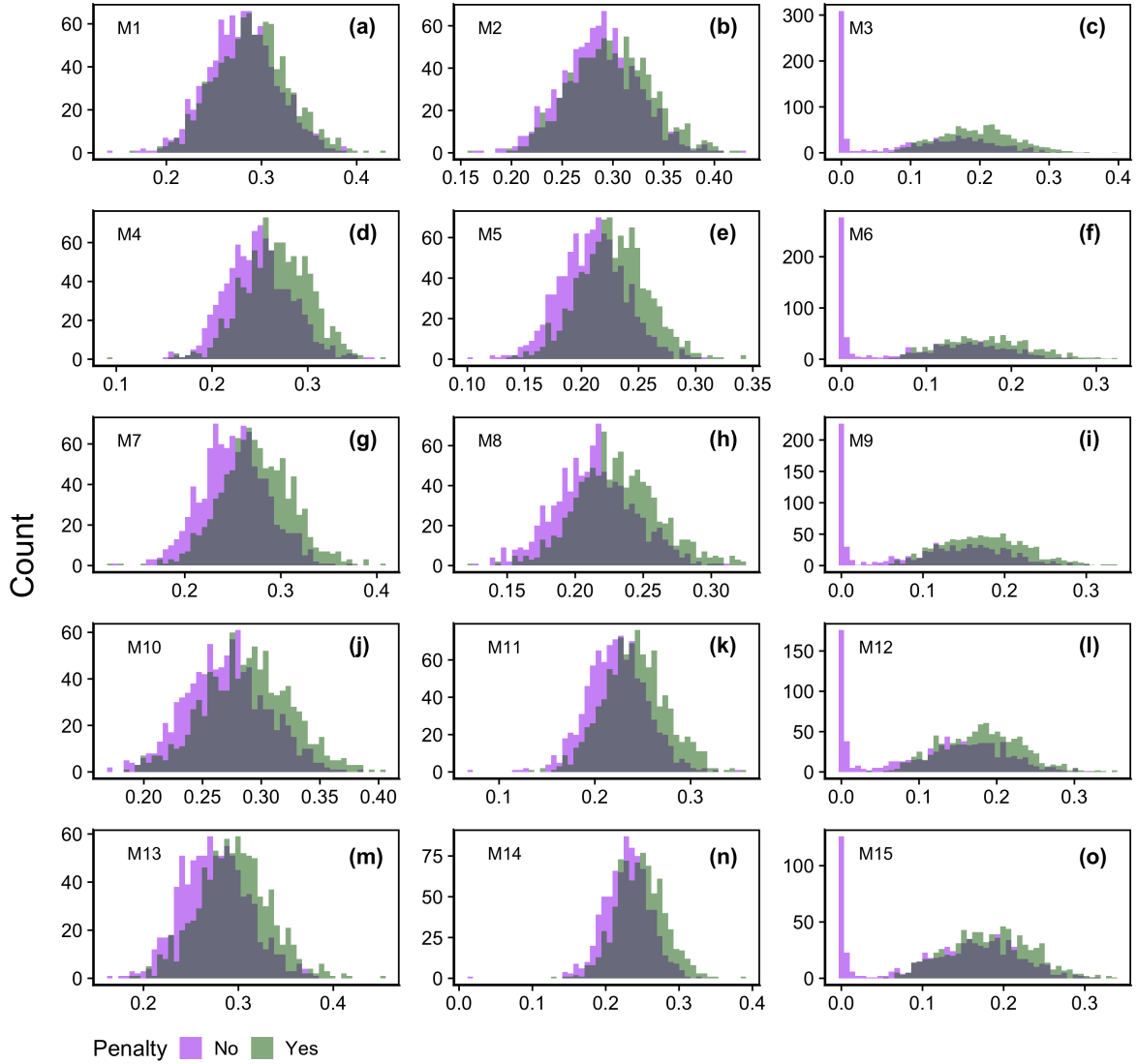


Fig. 8. Histograms of the estimated values of the standard deviation parameter for the observation error of the CPUE ($\hat{\sigma}_I$), with (dark green) and without (purple) the gamma penalty on the parameter. Each panel displays histograms of the parameter estimates from a different model, with the model name indicated in the top-left corner. The estimates were from the parametric bootstrap analysis.

Appendix A: Initial abundance

The abundance at near unfished equilibrium $N_{a,0}$ was calculated as:

$$N_{a,0} = \begin{cases} R, & \text{if } a = 0 \\ N_{a-1,0} \cdot e^{-Z_{a-1,0}}, & \text{if } 0 < a < A \\ \frac{N_{a-1,0} \cdot e^{-Z_{a-1,0}}}{1 - e^{-Z_{a,0}}}, & \text{if } a = A \end{cases}$$

The total mortality rate at equilibrium $Z_{a,0}$ consists of the age-specific fishing mortality rate at equilibrium $F_{a,0}$ and the constant natural mortality rate M (i.e., $Z_{a,0} = F_{a,0} + M$). $F_{a,0}$ was separated into two components: the fully selected fishing mortality rate F_0 and the age-dependent selectivity $S_{a,0}$. We assumed that the fishing mortality rate during the period before data collection was negligible and near zero, as the catch data for the initial years of the study period showed very low values. Therefore, the fully selected fishing mortality rate F_0 was fixed at 0.01, implying that $Z_{a,0} \approx M$, and the age-dependent selectivity $S_{a,0}$ was calculated using Equation (1), where $a_{05,t}$ was replaced with a_{05} .

Appendix B: CDF of a skew normal distribution

The cumulative distribution function (CDF) of a skew normal distribution $\Phi(\cdot)$ (Azzalini, 1985) to model the length-at-age distribution in catch was defined as

$$\Phi(x|\xi_a, \omega_a, \alpha_a) = \int_{-\infty}^x \left[\frac{1}{\xi_a \cdot \pi} \cdot e^{-\frac{(L-\xi_a)^2}{2\omega_a^2}} \cdot \int_{-\infty}^{\alpha_a \cdot \frac{L-\xi_a}{\omega_a}} e^{-\frac{t^2}{2}} dt \right] dL,$$

where a is the subscript for age, L is the length, x is the upper limit of integration over L , ξ_a is the location parameter, ω_a is the scale parameter, and α_a is the shape parameter.

Supplementary Material

Supplementary Tables

Table 6. Parameter lower and upper bounds, as well as initial values of parameters and random effects, for all alternative models fitted to the Korean mackerel data.

Quantity	Lower bound (l)	Upper bound (u)	Initial value
Parameter			
$\text{logit}_{(l,u)}(a_{05})$	0	2	0
$\text{logit}_{(l,u)}(a_{95})$	2	5	0
$\text{logit}_{(l,u)}(q_0)$	10^{-7}	10^{-2}	0
$\text{logit}_{(l,u)}(c)$	10^{-8}	10^{-2}	0
$\log(R)$	—	—	16
$\log(\sigma_R)$	—	—	0
$\log(\sigma_I)$	—	—	0
$\log(\sigma_F)$	—	—	0
$\log(\sigma_Y)$	—	—	0
$\log(\sigma_q)$	—	—	0
$\log(\theta)$	—	—	0
Random effect			
ε^R	—	—	0
ε^S	—	—	0
ε^F	—	—	0
ε^q	—	—	0

Table 7. Cross-test evaluation of AIC accuracy in model selection through 500 simulation-estimation runs for each combination of an operating Model (OM) and estimation model (EM). Rows indicate the OMs that simulated data, using parameter estimates from fitting the mackerel data as the true values. Columns represent the EMs applied to the simulated data. The table shows the frequency at which each EM was identified as the best model based on AIC. Numbers outside parentheses are from the cross-test where M12 imposed a gamma distribution penalty on the standard deviation parameter of the random walk catchability coefficient, denoted as σ_q . Numbers in parentheses represent outcomes where M12 did not apply the gamma distribution penalty to σ_q .

OM	EM			Total
	M10	M11	M12	
M10	400 (402)	50 (50)	0 (1)	450 (453)
M11	0 (0)	468 (466)	0 (1)	468 (467)
M12	167 (16)	186 (33)	1 (306)	354 (355)

Table 8. Coverage probabilities of the 95% confidence intervals for the fixed-effect parameters in all alternative models, based on 1000 runs of parametric bootstrap. The intervals were computed using the Wald interval.

Parameter	M1	M2	M3	M4	M5	M6	M7	M8	M9	M10	M11	M12	M13	M14	M15
$\log(R)$	95	91	93	94	93	92	93	93	92	93	93	93	94	91	93
$\text{logit}_{(0,2)}(a_{05})$	96	95	94	93	93	93	92	90	92	91	92	93	82	80	81
$\text{logit}_{(2,5)}(a_{95})$	95	94	95	95	95	95	96	95	96	95	95	96	95	95	96
$\log(\sigma_Y)$	92	92	91	92	92	88	90	90	87	91	92	89	89	93	88
$\log(\sigma_T)$	95	94	89	96	95	90	94	96	93	95	94	94	95	94	93
$\text{logit}_{(10^{-7}, 10^{-2})}(q_0)$	97	91	93	94	93	92	93	92	93	94	92	93	95	93	93
$\log(\sigma_F)$	94	93	95	94	95	94	94	93	95	93	94	96	93	95	94
$\log(\sigma_R)$	95	95	95	96	94	98	94	94	98	96	96	97	97	97	97
$\log(\theta)$	94	94	94	96	95	96	95	95	95	95	96	95	96	95	95
$\text{logit}_{(10^{-8}, 10^{-2})}(c)$	—	91	—	—	92	—	—	93	—	—	94	—	—	92	—
$\log(\sigma_q)$	—	—	95	—	—	98	—	—	97	—	—	96	—	—	96
$\log(\sigma_S)$	—	—	—	94	93	92	95	94	92	96	95	93	93	93	93

Supplementary Figures

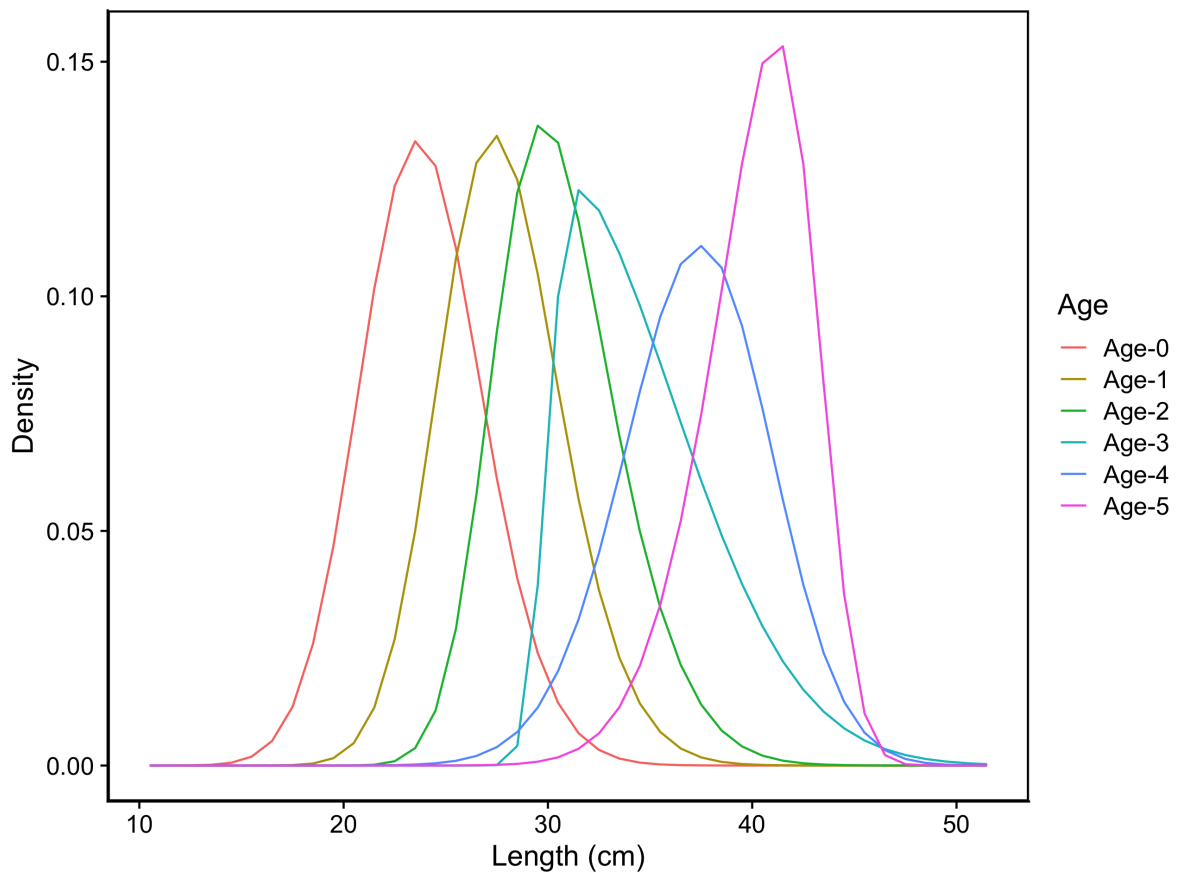


Fig. 9. Length-at-age distributions estimated using the minimum, mean, and maximum lengths at age from Jung et al. (2021a). The minimum and maximum lengths at age were employed to match the 5% and 95% percentiles of the skew normal distribution, respectively, while the mean length-at-ages were used to match the mean of each distribution.

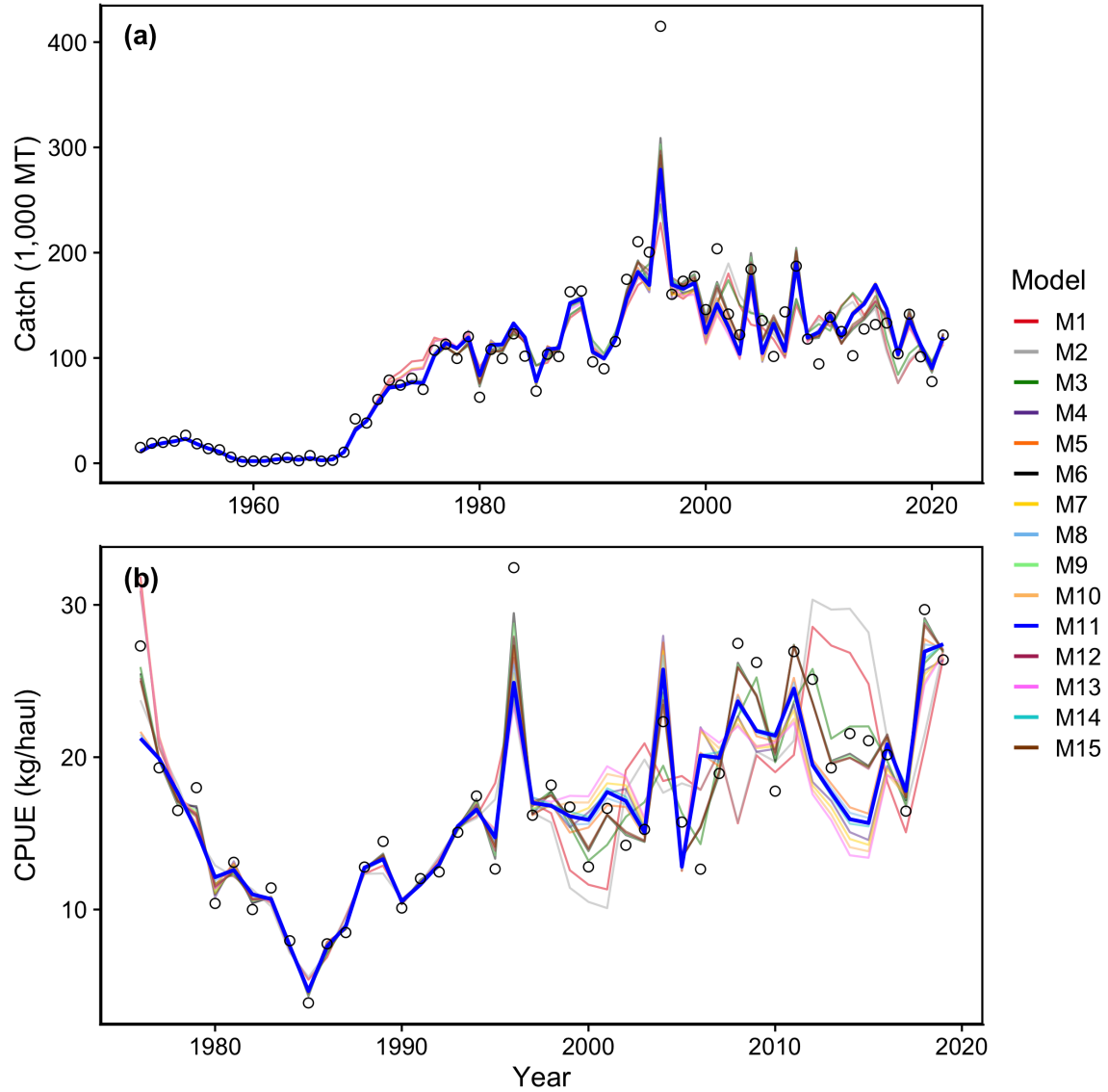


Fig. 10. Model-fitted values (solid lines) from all 15 alternative models and observed data (points) for the catch (a) and catch-per-unit-effort (CPUE) (b) data. Each color of the line represents a different model, and the blue line represents the best model (M11).

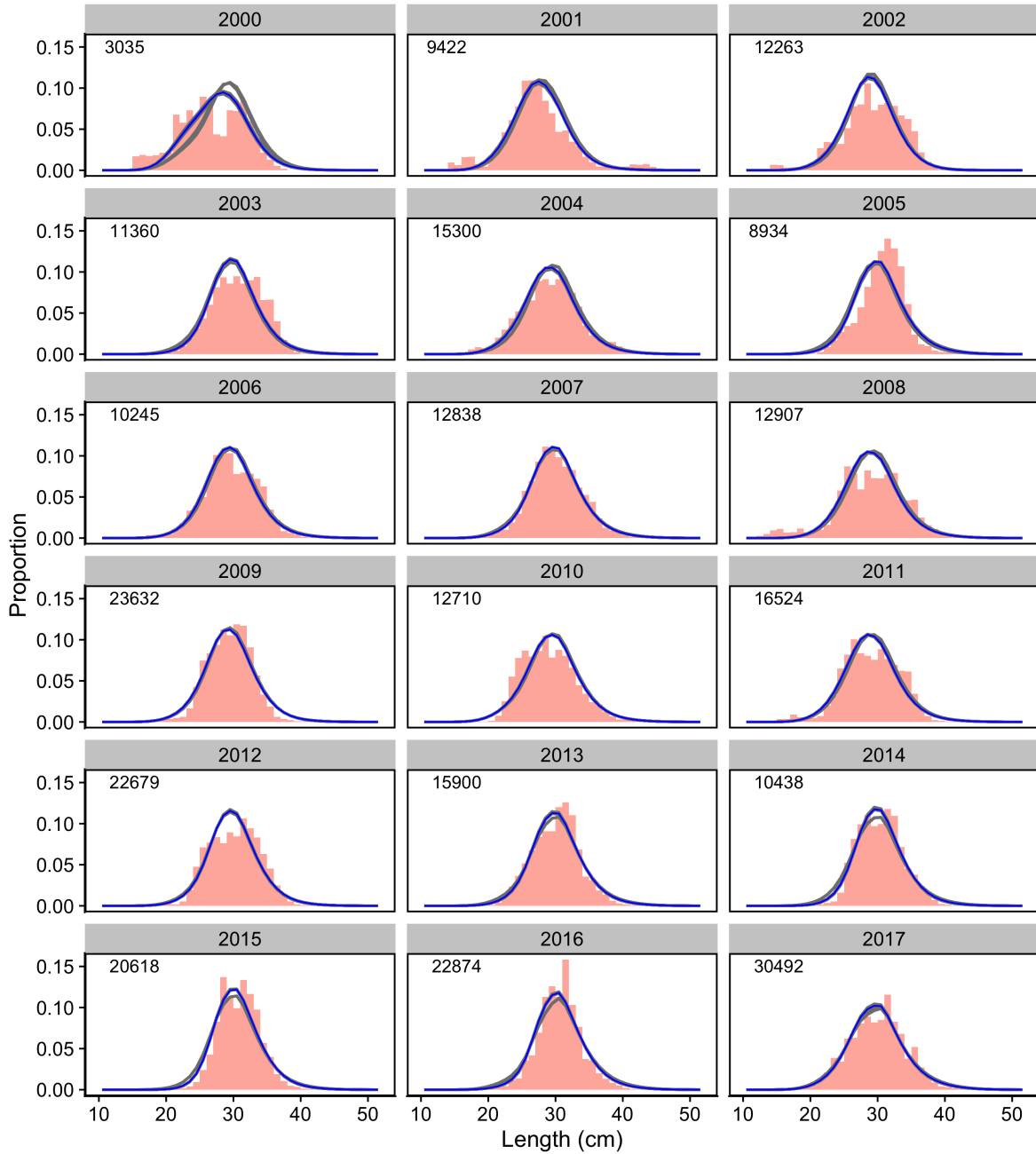


Fig. 11. Model-fitted values (solid lines) from all 15 alternative models and observed data (histograms) for the length composition data in proportion. Each line represents a different model, and the blue line represents the best model (M11). Each panel corresponds to a specific year, indicated in the top of each panel. The number of observations for each year is indicated in the top-left corner of each panel.

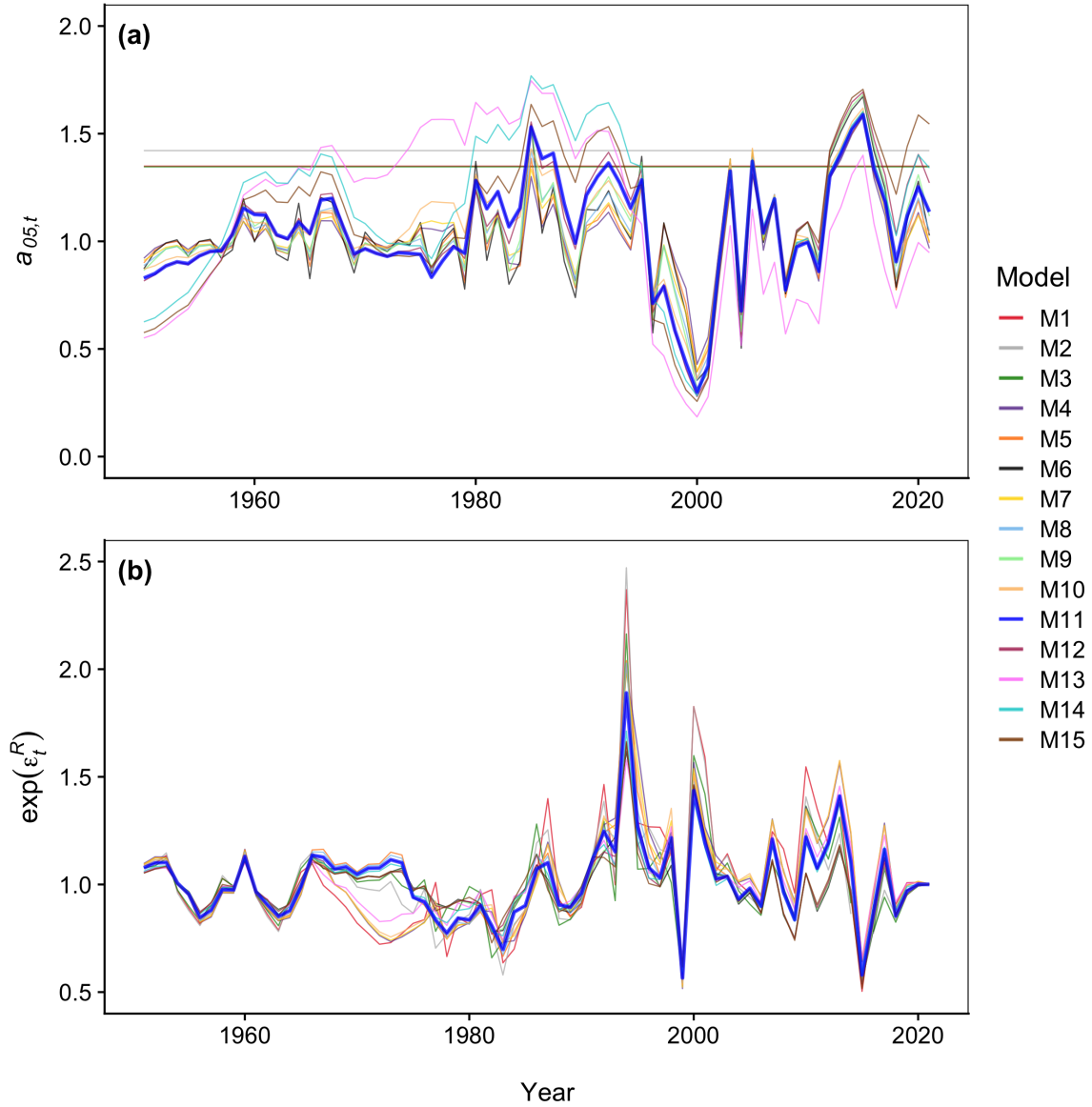


Fig. 12. Estimates of the time-varying age at 5% selectivity ($a_{0.5,t}$) (a) and those of the exponent of recruitment deviations ($\exp(\varepsilon_t^R)$) (b) from all 15 alternative models. Each color of the line represents a different model, and the blue line represents the best model (M11).

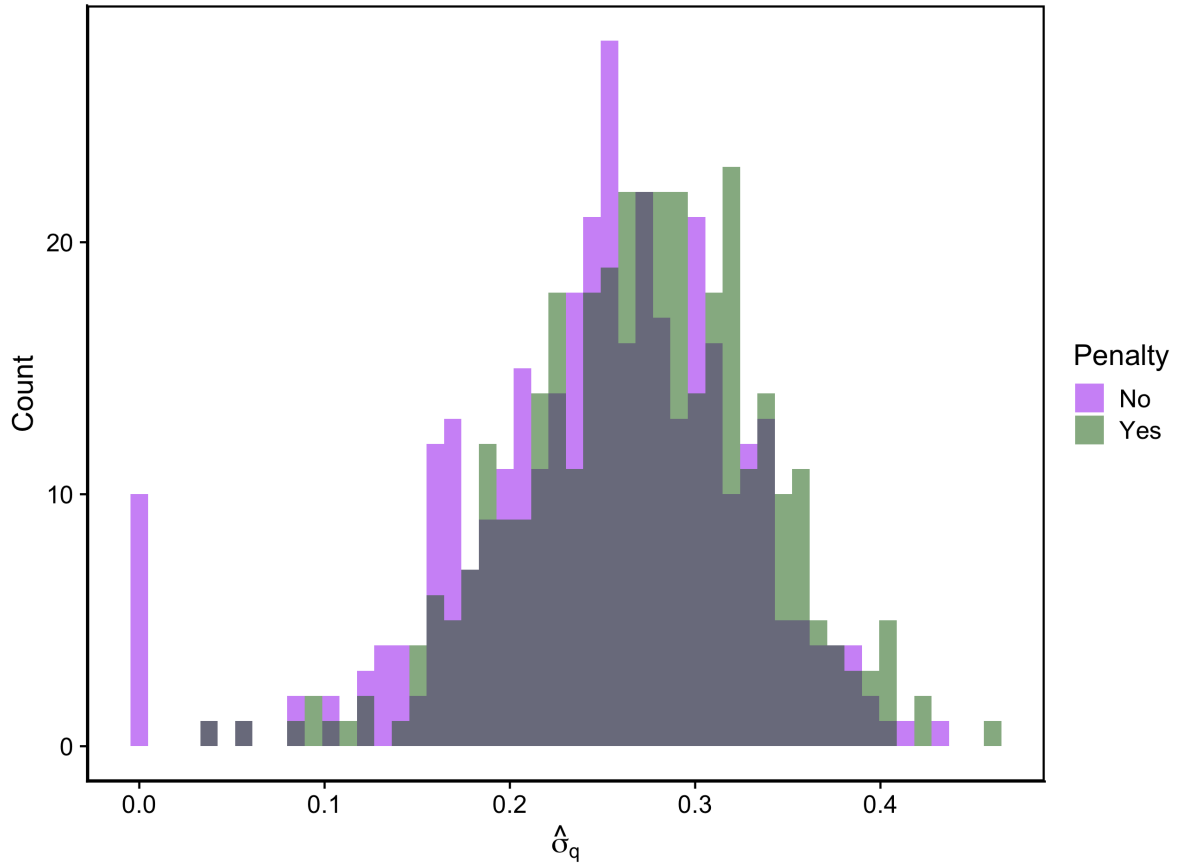


Fig. 13. Histograms of the estimates of the standard deviation parameter for the random walk catchability ($\hat{\sigma}_q$) in M12, with (dark green) and without (purple) the gamma penalty on the parameter.

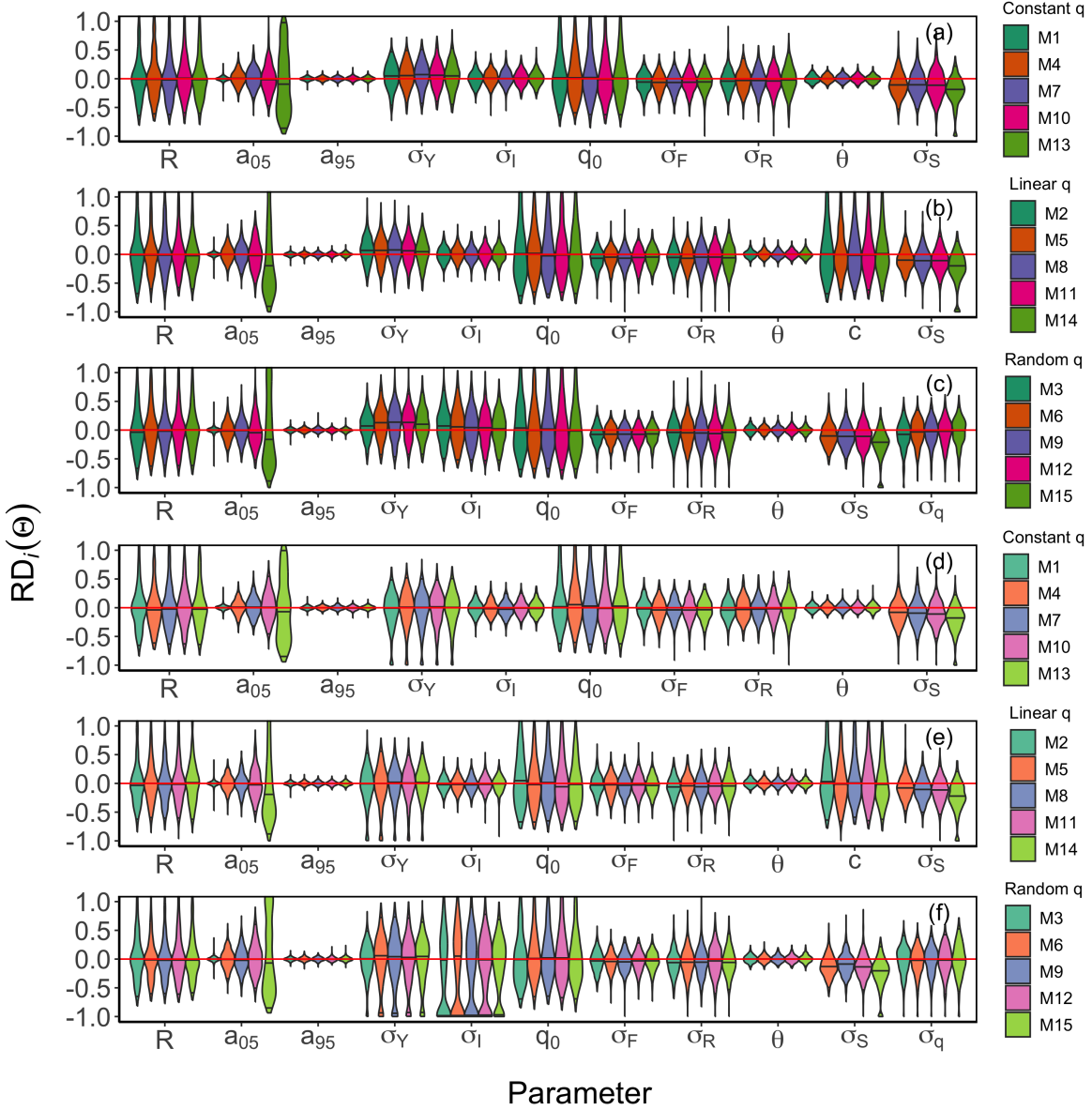


Fig. 14. Relative difference (RD) of the estimates of the fixed effect parameters for all alternative models (M1-15). The horizontal red line indicates no difference ($RD = 0$) between the estimates and their corresponding true values. The violin plots in each panel show the distributions of RD values from models under three catchability assumptions: constant catchability (a and d), linearly increasing catchability (b and e), and random walk catchability (c and f). Panels (a) to (c) display RD values for the estimates from models with gamma penalties on the standard deviation parameters, while panels (d) to (f) show RD values for estimates from models without gamma penalties on the standard deviation parameters. The horizontal lines within each violin plot indicate the 2.5%, 50%, and 97.5% percentiles of the RD values.

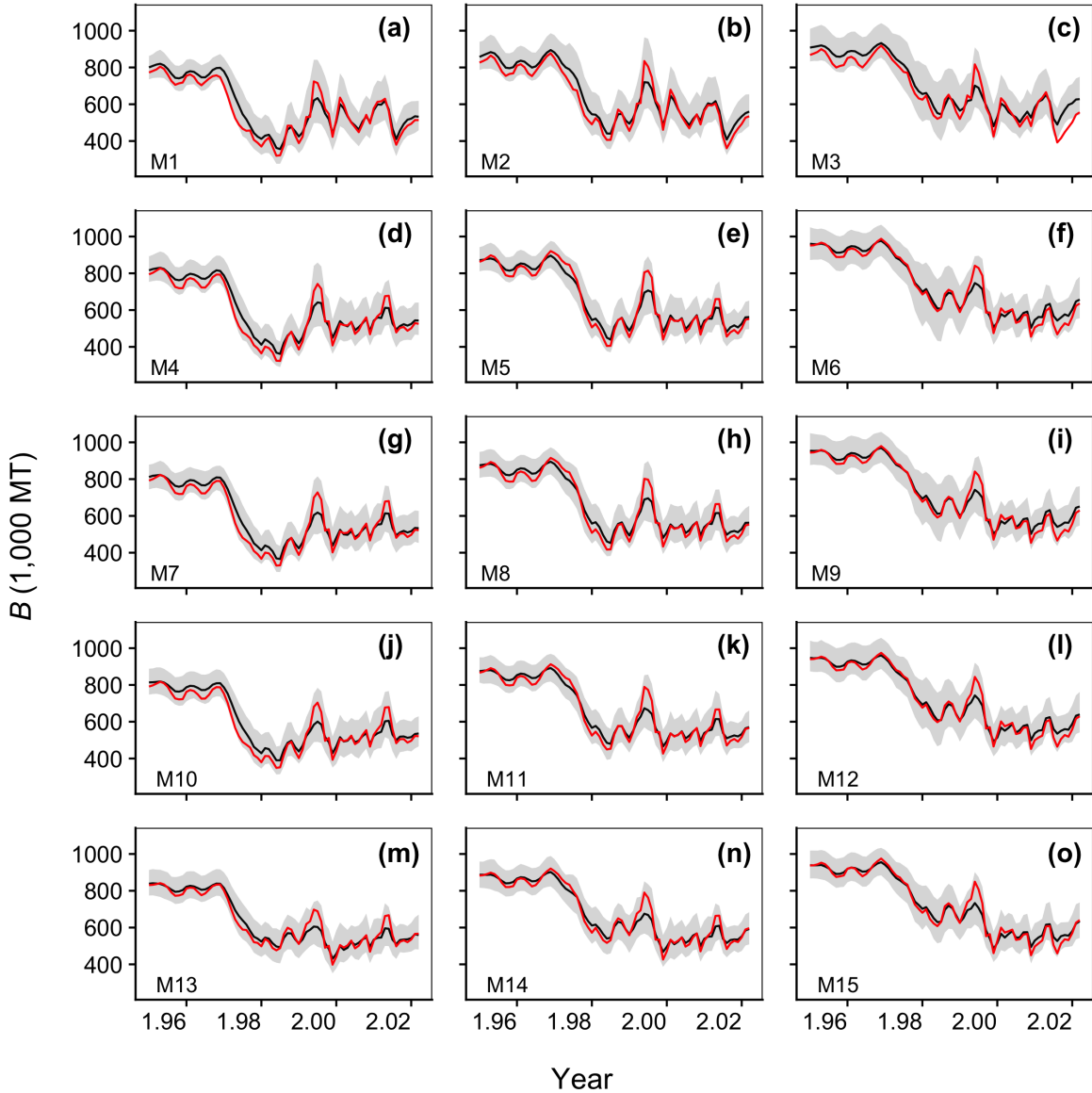


Fig. 15. Self-test estimates of the total biomass (B) and corresponding true values for all alternative models (M1-15), with the name of the corresponding model indicated in the bottom-left corner of each panel. The black lines indicate the median values of the self-test estimates, and the gray areas indicate the 95% intervals. The red lines indicate the true values.

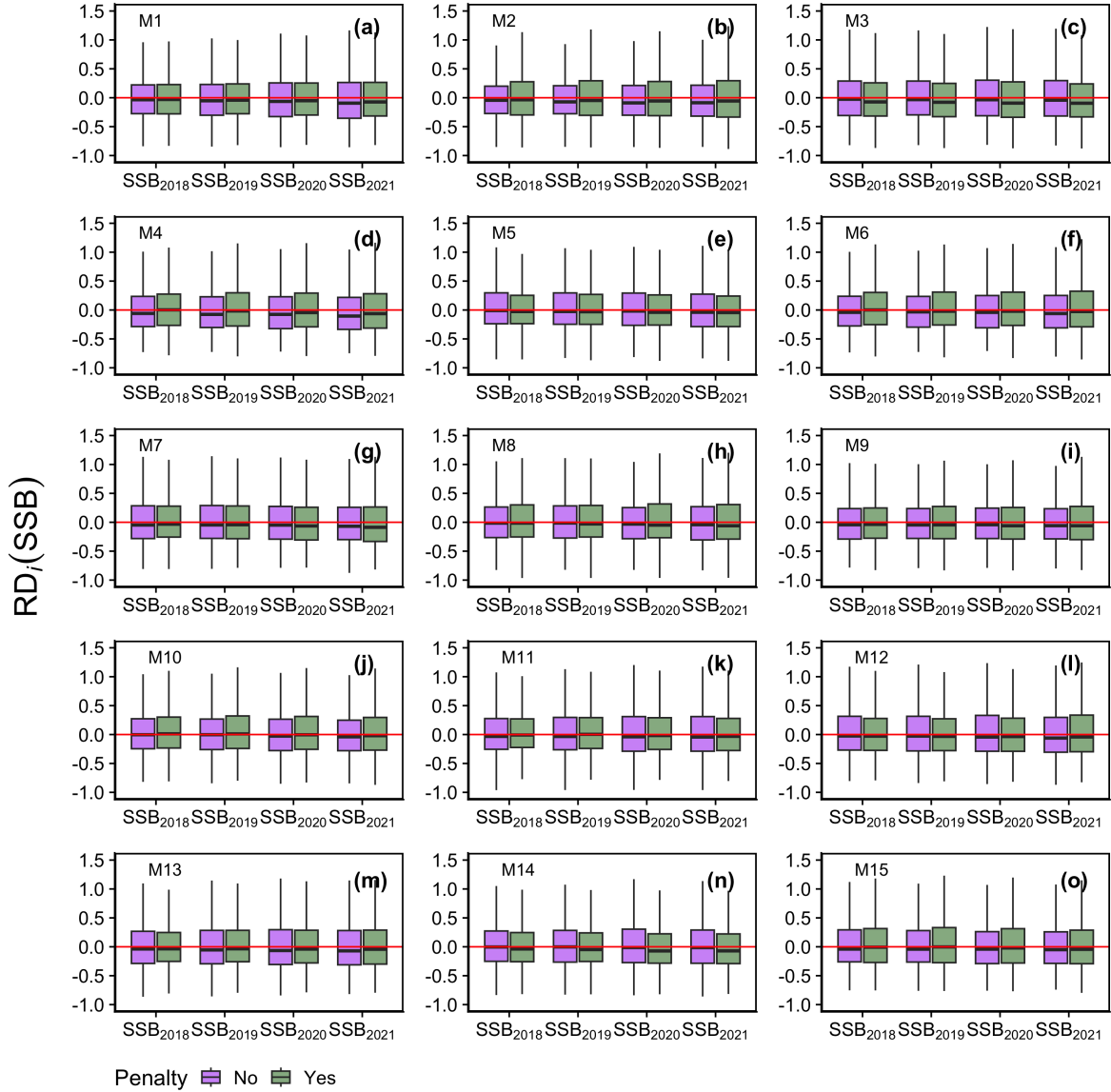


Fig. 16. Boxplots of the relative differences (RD) of the spawning stock biomass (SSB) for the last four years of the time series from all 15 alternative models (M1-15) compared to their corresponding true values. The horizontal red line indicates unbiasedness (i.e., $RD = 0$). Each panel corresponds to a different model, with the model name indicated in the top-left corner. Each colored boxplot represents the RDs from models with gamma penalties (dark green) and without gamma penalties (purple).

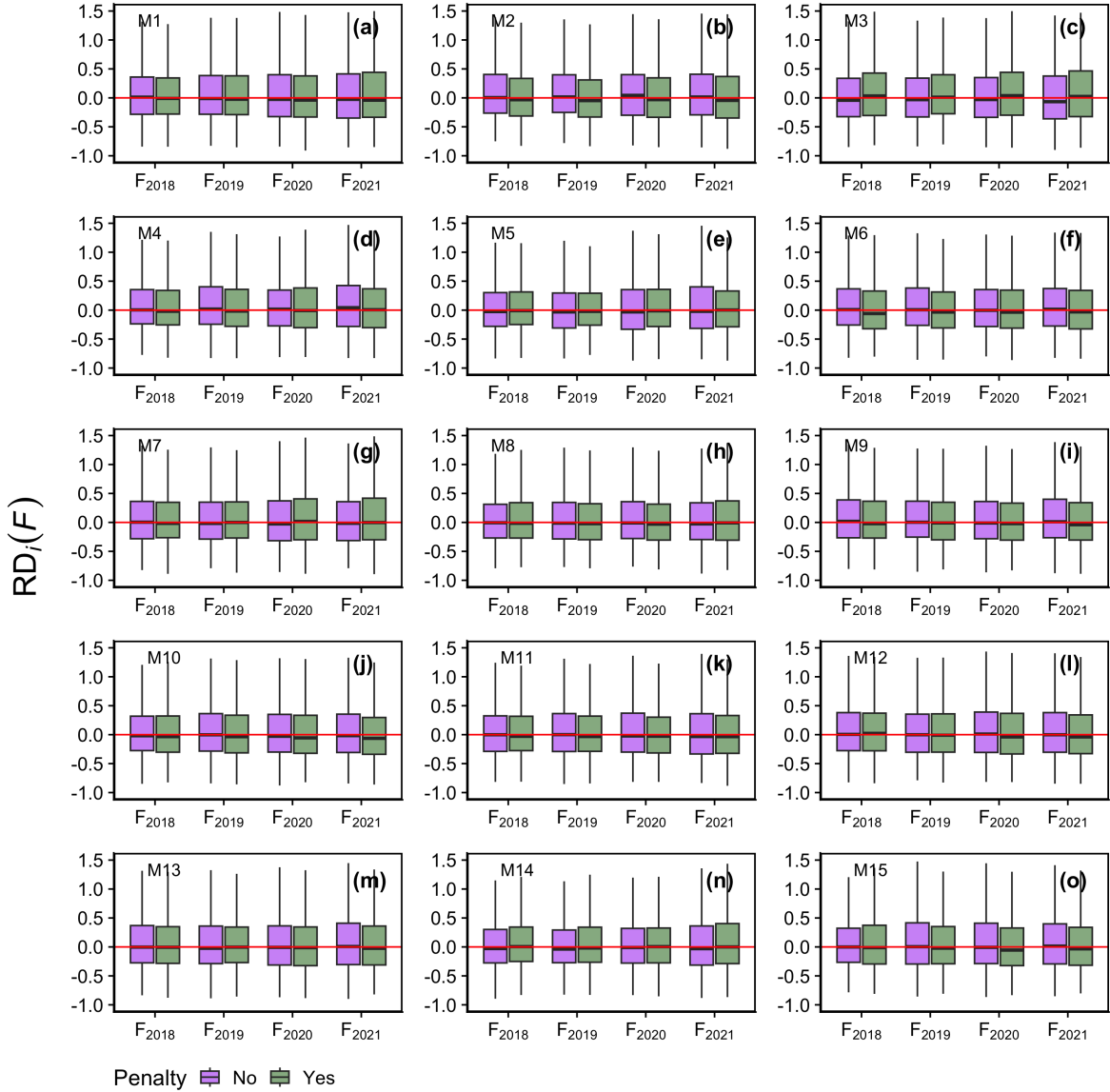


Fig. 17. Boxplots of the relative differences (RD) of the fishing mortality rate (F) for the last four years of the time series from all 15 alternative models (M1-15) compared to their corresponding true values. The horizontal red line indicates unbiasedness (i.e., $RD = 0$). Each panel corresponds to a different model, with the model name indicated in the top-left corner. Each colored boxplot represents the RDs from models with gamma penalties (dark green) and without gamma penalties (purple).

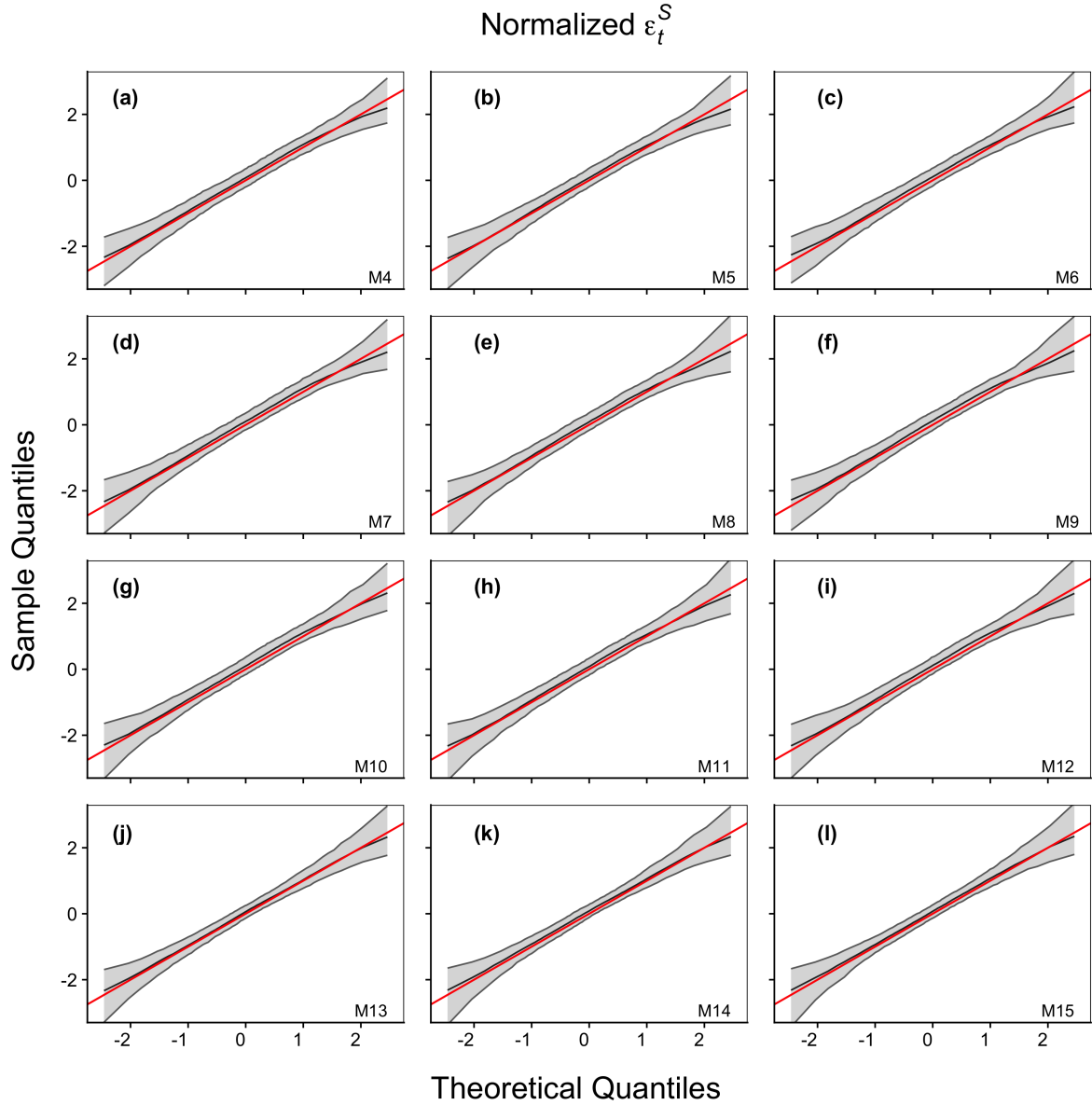


Fig. 18. Quantile-quantile (Q-Q) plots for the standardized samples of selectivity deviations for the time-varying age at 5% selectivity ($a_{05,t}$) in models assuming time-varying selectivity (M4-15). Each panel corresponds to a different model, with the model name indicated in the bottom-right corner. The diagonal red line serves as the reference for normality check. The 95% envelope of the Q-Q plot is shaded in gray, and the black line represents the median of the envelope.

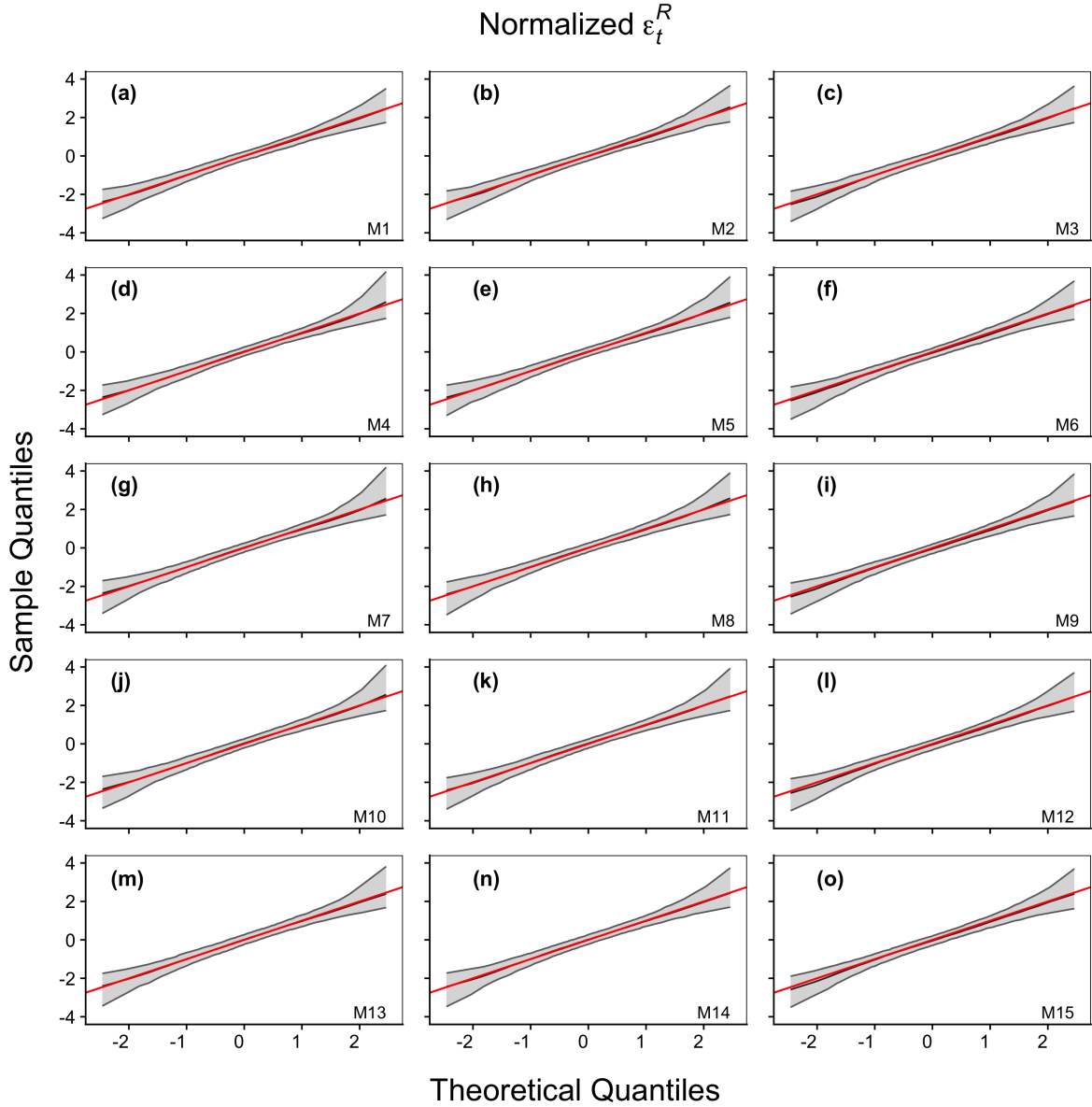


Fig. 19. Quantile-quantile (Q-Q) plots for the standardized samples of inter-annual deviations of the recruitment deviations from all alternative models (M1-15). Each panel corresponds to a different model, with the model name indicated in the bottom-right corner. The diagonal red line serves as the reference for normality check. The 95% envelope of the Q-Q plot is shaded in gray, and the black line represents the median of the envelope.

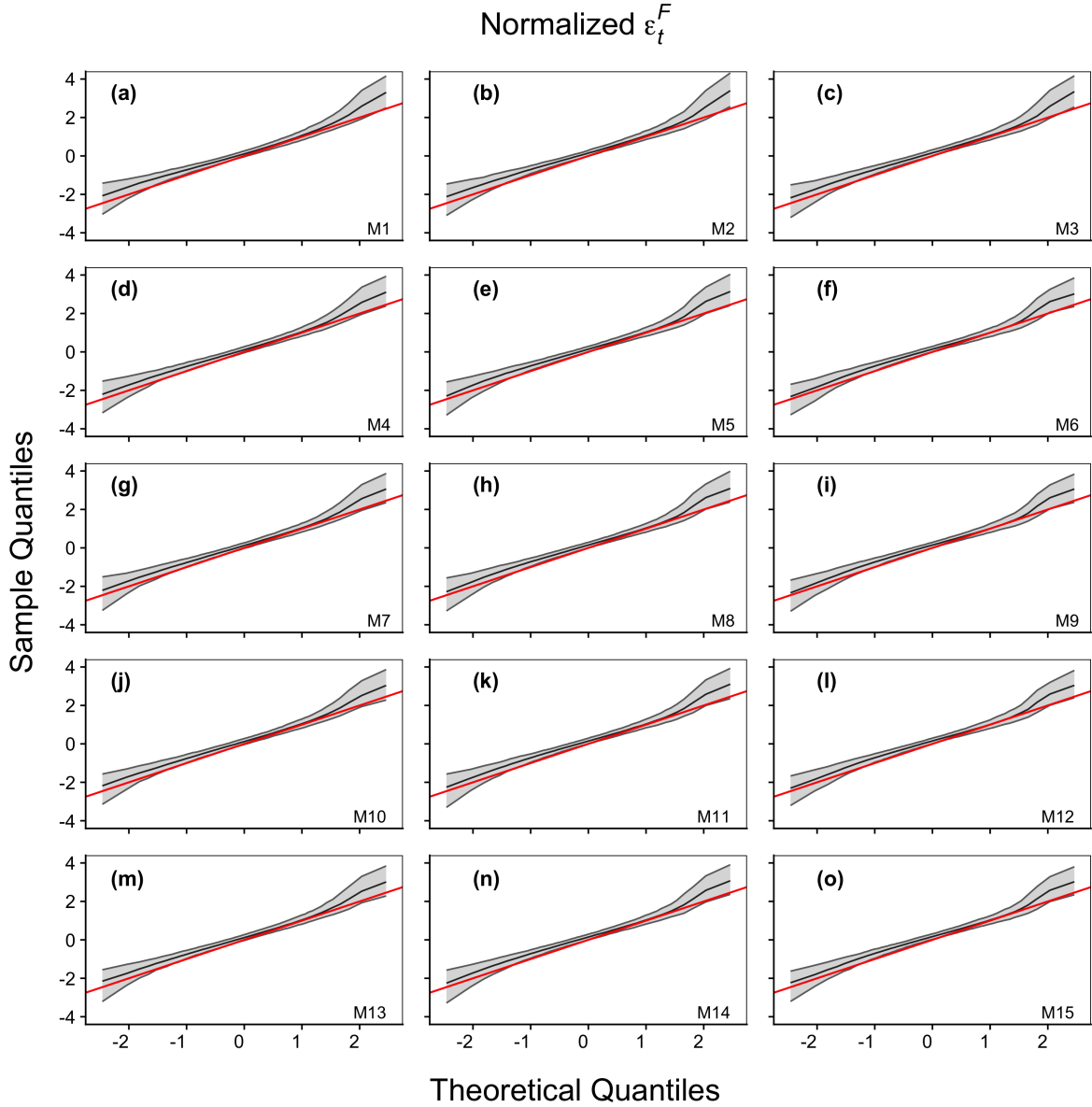


Fig. 20. Quantile-quantile (Q-Q) plots for the standardized samples of inter-annual deviations of the fishing mortality rates in log-scale from all alternative models (M1-15). Each panel corresponds to a different model, with the model name indicated in the bottom-right corner. The diagonal red line serves as the reference for normality check. The 95% envelope of the Q-Q plot is shaded in gray, and the black line represents the median of the envelope.

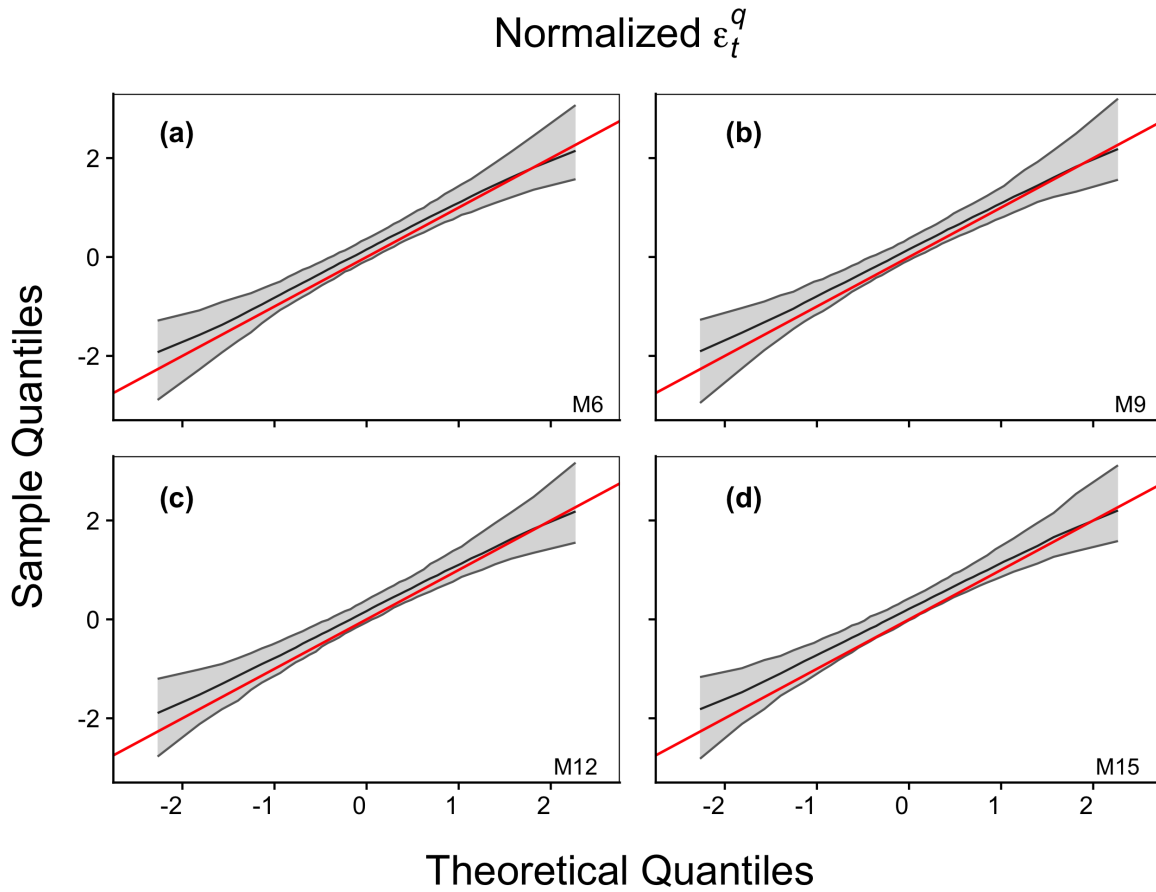


Fig. 21. Quantile-quantile (Q-Q) plots for the standardized samples of inter-annual deviations of the catchability in log-scale from models assuming random walk catchability (M6, M9, M12, M15). Each panel corresponds to a different model, with the model name indicated in the bottom-right corner. The diagonal red line serves as the reference for normality check. The 95% envelope of the Q-Q plot is shaded in gray, and the black line represents the median of the envelope.